TAILORING THE ASSEMBLY OF GRAPHENE MATERIALS IN WATER-BASED WET SPINNING PROCESS

A Thesis

Presented to the Faculty of the Graduate School

of Cornell University

In Partial Fulfillment of the Requirements for the Degree of

Master of Science

by

Chao-Wen Chang

August, 2019

ABSTRACT

Graphene is one of the most attractive carbon-based materials due to its extraordinary material properties originating from the atomically single- or small-number-layered structure. Integration of 2D graphene sheets into macroscopic architectures such as fibers illuminates the probability to transfer the excellent properties of individual graphene into advanced 3D ensembles for promising applications. However, the lack of effective, low-cost and convenient assembly strategy has blocked its further development. Therefore, water-soluble graphene oxide (GO), an oxidized form of graphene, is an alternative precursor for building 3D frameworks. Herein, we demonstrate that neat and macroscopic GO fibers can be easily fabricated through wet spinning technique. The self-assembled fibers further undergo intense thermal reduction and form neat graphene fibers. Surprisingly, the electrical and thermal conductivity of these graphene fibers is found to be much higher than polycrystalline graphite and other types of 3D carbon-based materials without sacrificing mechanical strength which can be applied to capacitors and energy storage devices.

In addition, this one-step spinning technique can be applied to the transportation and storage of graphene oxide. GO is commonly synthesized in water by Hummers' method and should be transported in water dispersion. Moreover, in the solution-based synthesis, GO suffers from severe restacking between individual sheets and thus loses its material identity and advantages. With the help of wet spinning, GO water suspension smartly extracts into dense fibers, which is much easier to handle compared to bulky water bottles and then bring down the transportation cost. We introduce sodium hydroxide as a coagulation agent to rapidly acquire GO fibers without restacking as well as altering its liquid crystallinity.

BIOGRAPHICAL SKETCH

Chao-Wen Chang was born in Taipei, Taiwan, on July 4, 1994. His interest in science and nature was intrigued at early as during elementary school. He attended National Taiwan University and majored in chemical engineering in 2012, hoped to combine the knowledge of chemistry and physics. After graduation in 2017, Chao-Wen moved to United States to pursue his Master of Science degree at Cornell University in order to navigate the enormous ocean of science as well as expanding horizon. At Cornell University, he chose Professor Yong L. Joo as his advisor and studied to work as a researcher developing novel self-assembled wet-spun graphene oxide fibers and their applications.

ACKNOWLEDGEMENTS

I would like to thank my advisor Professor Yong L. Joo for his patient guidance, encouragement and advice through the learning process of my master program. I have learned to become a more efficient but rigorous researcher. I would also like to thank my committee member Prof. Juan Hinestroza for his valuable inputs and suggestions.

I would also like to thank to Dr. Somayeh Zamani, Mani Modayil Korah for their help on my project, and the rest of the Joo group members for their kind help and valuable suggestions academically, experimentally and mentally.

Finally, I would like to express my sincere gratitude to my parents for their mental and financial support in my whole life and for the precious chance to study here in Cornell University. Without them, I would not become who I am.

Contents

CHAPTER 1

Introduction

1.1 Overview of Carbon Fiber

The creation of carbon fiber (CF) can be traced back to the pyrolysis of natural cellulose fibers for electrical-light bulbs by Sir Joseph Swan in 1883. CF became widely attractive when teams at the Royal Aircraft Establishment and Rolls Royce, Ltd., promoted CF to a high-performance fiber with extraordinary mechanical strength (1.7 GPa) and tensile modulus (400 GPa) in the 1960s[1,2]. This almost purely carbonaceous fiber is usually prepared from natural cellulose, synthetic polyacrylonitrile (PAN) and pitch, by carbonization or graphitization at high temperatures to eliminate other chemical elements/functional groups and generate graphitic structures[3,4]. The first attractive characteristic of CFs is the extraordinary mechanical properties. The combination of high tensile strength and elastic modulus along with their light weight means they overwhelm steel in enforcement applications as structural components like transportation vehicles, civil engineering, aerospace and sport goods. Beyond its outstanding mechanical strength, CFs possess a wealth of additional functionalities such as favorable resistance to chemicals and harsh surroundings, and stability at high temperature. However, CFs has electrical conductivities in a very wide range[5–8] as well as thermal conductivities[9,10] due to the adulteration of epoxy or other components. Therefore, other forms of carbon-based fiber are urgent to be proposed. Table 1 shows some common CFs' basic properties.

Precursor	Tensile Strength (GPa)	Tenacity (cN/tex)	Young's Modulus (GPa)	Elongation at break (%)
PAN	2.5-7.0		250-400	0.6-2.5

Mesophase pitch	1.5-3.5		200-800	0.3-0.9
Rayon	≈1.0	23.9	≈50	≈2.5
Lyocell		40.2		13.0
Fortisan		23.9		3.2
Cupro		22.3		24.3
Bocell		38.2		9.7

Table 1. Axial mechanical properties of common fibers[3,11]. Fortisan, Cupro, and Bocell are all cellulose-based fiber. Fortisan is saponified cellulose acetate fiber. Cupro fibers regenerated from an aqueous solution in $[Cu(NH_3)_4](OH)_2$. Bocell fibers regenerated from a phosphoric acid solution and spun by an airgap spinning process.

Fabrication of carbon nanotube (CNT) fibers has been attracting tremendous attention for years with the desire to integrate such unique properties as high strength, electrical and thermal conductivities of the individual nanotubes into the useful, macroscopic ensembles. Breakthroughs have been made in wet approaches and dry-state spinning of CNTs for fiber fabrication. CNT is the typical one-dimensional (1D) nanostructure with high aspect ratio and strong binding force between its bundles. As a result, CNT fibers and sheets can be directly drawn out from their arrays or high concentration suspensions. However, beyond the superb properties of as-produced CNT fibers, the high cost for producing the initial super-aligned CNT arrays is inevitable[12,13], and extremely strict conditions such as high temperature (usually higher than 1000 °C)[14], and caustic media (e.g. super strong acid like fuming sulfuric[15] acid and chlorosulphonic acid[16]) for CNT dispersion are drawbacks of CNT fiber fabrication. The preparation of such fibers containing only CNTs is still a big challenge.

Graphene, a two-dimensional (2D) monolayer of carbon atoms, also possesses extremely high electrical, thermal and mechanical properties owing to their sp^2-bonding and nearly defect-free structure[17]. The more detailed introduction of graphene fiber is in Chapter 2. To conclude, both graphene fiber and CNT fiber can almost preserve the superb properties of pure graphene or CNT which have excellent conductivities despite of the relatively poor mechanical strength compared to CFs.

Although CNTs and graphene have super high conductivities and mechanical strength, they are poorly dispersed in water or common polar solvents that obstruct the processability and direct assembly to 3D architecture. Alternatively, graphene oxide (GO) with abundant of oxygen functional groups on its basal planes and edges possess advantages such as good solubility, easy handle, and scalable production with low cost improve the chances in assembling 2D sheets into macroscopic graphene-based architectures. Further chemical reduction down to reduced graphene oxide (rGO) or graphene is currently seen as the most suitable method of massive production of graphene. GO is usually synthesized from graphite using modified Hummer's method. One of the most important feature of GO solution is its liquid crystallinity (LC). Concentration and aspect ratio, which is lateral size over thickness, are two decisive factors of forming LCs. Higher concentration or higher aspect ratio increase the probability to turn GO from isotropic to nematic, which further facilitate the super-alignment of GO gel solution.

1.2 Overview of Wet-Spinning Process

This process is used for polymers or other fiber-forming materials that need to be dissolved or dispersed in a solvent (usually non-volatile) to be spun. The spinneret is submerged in a chemical

bath/coagulation medium that causes the fiber to precipitate, and then solidify, as it emerges. The fibers are then washed and dried. Finally, the filament yarn either is immediately wound onto bobbins or is further treated for certain desired characteristics or end use. During the coagulation and washing process, the fiber experiences elongation with certain tension force to strengthen and densify the structure. Figure 1.1 shows the schematic of how wet-spinning process is performed. The process gets its name from this "wet" bath. Acrylic, Rayon, Aramid, and Spandex are produced via this process. For example, Rayon fabric is made by cellulose using sulfuric acid and sodium sulfate as coagulant and aqueous solution with sodium salt as solvent. Spandex is a polyurethane fiber fabricated using Dimethylformamide as coagulation bath.

A variant of wet spinning is dry jet-wet spinning, where the solution is extruded into air and drawn, and then submerged into a liquid bath. Dry spinning includes a solution consisting of a fiber-forming material and a volatile solvent. The solution is extruded through a spinneret. A stream of hot air impinges on the jets of solution emerging from the spinneret, the solvent evaporates, and solid filaments are left behind.

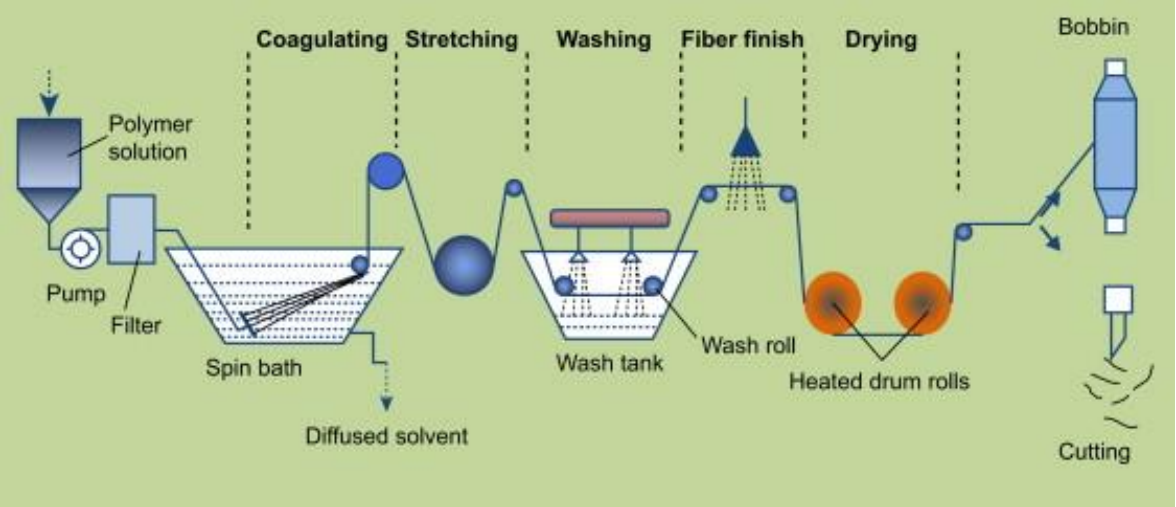

Figure 1.1 Schematic of wet-spinning process[17].

REFERENCES

[1] W.W.& W.J. R. MORETON, Carbon Fibres of High Strength and High Breaking Strain, Nature. 213 (1967) 690–691.

[2] A. E. STANDAGE & R. PRESCOTT, High Elastic Modulus Carbon Fibre, Nature. 211 (1966) 169.

[3] E. Frank, L.M. Steudle, D. Ingildeev, J.M. Spçrl, M.R. Buchmeiser, Carbon Fibers : Precursor Systems , Processing , Structure , and Properties Angewandte, Angew. Chemie Int. Ed. 53 (2014) 5262–5298. doi:10.1002/anie.201306129.

[4] R. Jeffries, Prospects lor carbon Fibres, Nature. 232 (1971) 304–307.

[5] S. Yao, F. Jin, K. Yop, D. Hui, S. Park, Recent advances in carbon- fi ber-reinforced thermoplastic composites : A review, Compos. Part B. 142 (2018) 241–250. doi:10.1016/j.compositesb.2017.12.007.

[6] D. Wentzel, I. Sevostianov, EFFECT OF FIBER DAMAGE ON THE OVERALL ELECTRICAL CONDUCTIVITY OF, Lett. Fract. MICROMECHANICS. 183 (2013) 275–282. doi:10.1007/s10704-013-9880-x.

[7] S.A. Jawad, M. Ahmad, Y. Ramadin, A. Zihlifl, V. Toiano, A.F. Na, Electrical Properties of Laminated Epoxy-Carbon Fiber Composite, Polym. Int. 32 (1993) 23–31.

[8] C.N. Owston, Electrical properties of single carbon fibres, J. Phys. D. Appl. Phys. 3 (1970) 1615.

[9] D.J. Radcliffe, H.M. Rosenberg, The thermal conductivity of glass-fibre and carbon-fibre/epoxy composites from 2 to 80 K, Cryogenics. (1982) 245–249.

[10] M.A.B. M. W. PILLING, B. YATES, The thermal conductivity of carbon fibre-reinforced composites, J. Mater. Sci. 14 (1979) 1326–1338.

[11] S. Chand, Carbon fibers for composites, J. Mater. Sci. 35 (2000) 1303–1313.

[12] M. Zhang, Zhang , M ., Atkinson , K . R . & Baughman , R . H . Multifunctional carbon nanotube Multifunctional Carbon Nanotube Yarns by Downsizing an Ancient Technology, Science. (2015) 1358–1361. doi:10.1126/science.1104276.

[13] Q.L.& S.F. Kaili Jiang, Spinning continuous carbon nanotube yarns, Nature. 419 (2002) 1274014.

[14] Y. Li, I.A. Kinloch, A.H. Windle, Direct Spinning of Carbon Nanotube Fibers from Chemical Vapor Deposition Synthesis, Science. 304 (2004) 276–278.

[15] L.M. Ericson, H. Fan, H. Peng, V.A. Davis, W. Zhou, J. Sulpizio, Y. Wang, R. Booker, J. Vavro, C. Guthy, A.N.G. Parra-vasquez, M.J. Kim, S. Ramesh, R.K. Saini, C. Kittrell, G. Lavin, H. Schmidt, W.W. Adams, W.E. Billups, M. Pasquali, W. Hwang, R.H. Hauge, J.E. Fischer, R.E. Smalley, Macroscopic , Neat , Single-Walled Carbon Nanotube Fibers, Science. 305 (2004) 1447–1451.

[16] V.A. Davis, A.N.G. Parra-vasquez, M.J. Green, P.K. Rai, N. Behabtu, V. Prieto, R.D. Booker, J. Schmidt, E. Kesselman, Y. Talmon, R.E. Smalley, M. Pasquali, True solutions of single-walled carbon nanotubes for assembly into macroscopic materials, Nat. Nanotechnol. (2009). doi:10.1038/nnano.2009.302.

[17] R. Alagirusamy, A. Das, Conversion of Fibre to Yarn, Elsevier Ltd, 2014. doi:10.1016/b978-1-84569-931-4.00008-8.

CHAPTER 2

Facile and Scalable Fabrication of Wet-spun Self-assembled Graphene Oxide Fiber

2.1 Introduction

Graphene is a two-dimension (2D) monolayer carbon atoms tightly packed into a honeycomb lattice, which has attracted persistent attention from scientists during the past decades. It is also the fundamental building block of all the graphitic materials. The intriguing electronic, thermal, and mechanic properties mainly arise from its truly atomic thickness along with strictly 2D, sp^2-hybridized carbon structure[1], and therefore bring about the greatly promising applications in electronic and energy storage devices[2], sensors[3][4], catalysis[5][6], composites[6] and so on. Nowadays, translation of the individual property of the graphene sheets into the macroscopic, ordered materials are without doubt an extraordinarily hot and useful topic in view of exploring advanced properties of 2D graphene sheets for practical applications. Plenty progresses have demonstrated that graphene sheets can be assembled into 2D macroscopic thin films, and 3D composites with polymers via various methods and techniques. However, in most cases, the limited dispersibility of graphene sheets in common solvents hinders the development of the direct assembly of graphene sheets.

Alternatively, highly water-soluble graphene oxide (GO) with abundant oxygen functional group on its basal planes and edges is easily processable in water or hydrophilic solutions. And then it can be chemically or thermally converted into graphene. The advantages of GO, such as good solubility, easy handle, and scalable production with low cost improve the chances in assembling 2D sheets into macroscopic graphene-based architectures.

The discovery of anisotropic liquid crystalline (LC) behavior of graphene oxide dispersions[7][8] in various organic and aqueous media leads to a pre-aligned orientation which can further be directed under shear flow to form an ordered assembly of nanocomponents into macroscopic structures via simple, fast, and cost-effective methods like wet-spinning process.

Cong et al. was the first team who used CTAB as coagulation agent for making self-assembled GO fiber[9]. Jalili et al. tried many coagulants for in situ wet-spinning GO fibers and found out that chitosan and calcium chlorite performed the best[10]. Xu et al. used giant GO fiber to form chemically reduced graphene fiber with Ca^{2+} as crosslinking agent which had high mechanical strength (501 MPa) and electrical conductivity (4.1×10^4 S/m)[11]. Xin et al. reported even higher mechanical strength (1005 MPa), electrical conductivity (1.79×10^5 S/m), and thermal conductivity (1025 W/m-K) for thermally reduced graphite fibers[12]. Some other strong graphene-based fiber with high stiffness and elasticity have been fabricated[13]. GO- or rGO-modified carbon or polymer fiber composite or have been further proposed and fabricated to ameliorate interfacial shear strength and toughness[14][15]. Some other applications include self-healing GO-polyurethane composite fiber[16] and 2-dimensional non-woven GO fabric[17].

Herein, our group has raised a wet-spinning methodology to fabricate neat graphene fibers from concentrated GO liquid crystal, and the curliness-fold formation mechanism of GO fiber has been proposed. Compared with the composite fibers or carbon fiber, the neat graphene fibers demonstrated several orders of magnitude higher electrical conductivity but relatively lower strength. Therefore, we introduced large GO sheets (average size = 57 μm) as the building block

to achieve extraordinarily high electrical and thermal conductivity and good mechanical strength. Generally, greater aspect ratio of building blocks and their better alignment in the fiber axis are the main factors to improve the mechanical properties of polymer fibers. Inspired by this concept, we employed relatively large GO sheets with extremely high aspect ratios as building blocks to reduce defective edges and achieved highly ordered alignment of GO to make high-performance graphene/graphite fibers with both high strength and conductivity. Furthermore, after thermal reduction, the GO fibers turned into graphite fibers, which exhibited extremely high electric and thermal conductivity with comparably high tensile strength.

2.2 Experimental Methods

2.2.1 Materials

Graphene oxide aqueous solution was purchased from EMD Performance Materials Corp. Hexadecyltrimethylammonium bromide (CTAB) (>98%) and calcium chloride (>97%) were purchased from Sigma-Aldrich. Ethyl alcohol (>99%) was purchased from VWR Chemicals.

2.2.2 Fabrication of Graphene Oxide Fibers

2 wt.% of degassed GO dispersion in water was sonicated for 30 minutes and then loaded in a plastic syringe and injected into a rotating CTAB coagulation bath (15 rpm) with the infusion rate of 5 ml/min. A steel needle (22 gauge) was placed after the plastic syringe to create volume confinement. The coagulation bath consisted of 1:1 volume ratio of water and ethanol, and CTAB concentration is 0.5 mg/ml. The obtained fibers remained in the bath for 30 min before winding around a Teflon bar, and then soaked the bar in a washing bath (1:1 volume ratio of water and ethanol) for another 40 min. The fibers then were unwound. Finally, the washed fibers were wound on a graphite bar and dried in air with generated tension within the fiber.

2.2.3 Heat Treatment Process

The graphite bars with GO samples wound on it were put in the MTI Furnace under 400 °C for 1 hour with 3 °C/min heating ramp rate in 95% argon/5% hydrogen atmosphere. This is reduced graphene oxide sample is now called rGO_{400}. GO samples rGO_{400} then underwent high temperature annealing in Material Research Furnace LLC, NH. GO fibers first underwent 1200 °C for 2 hours and then experienced 2500 °C for 30 minutes with 10 °C/min ramp rate, all under Argon atmosphere. This greyish sample is called $rGO_{1200,\ 2500}$ fiber. rGO_{400} fiber underwent 2500 °C for 30 minutes with 10 °C /min ramp rate under Argon atmosphere, which is called $rGO_{400,\ 2500}$ fiber.

2.2.4 Characterization Methods

The morphology and microstructure of the fibers were characterized by a field-emission scanning electron microscope (SEM) LEO (Zeiss) 1550. X-ray diffraction (XRD) patterns of oxidized graphite synthesis were determined by a D8 Advance ECO powder diffractometer (Bruker Corporation) using a high-brilliance 1 kW X-ray source. The Fourier transformed infrared (FTIR) spectrum was measured with a PerkinElmer Frontier MIR Spectrometer coupled with a $LiTaO_3$ MIR detector in the range of 600−4000 cm^{-1} with 32 scans for each sample. The microstructures of graphene oxide sheets were investigated using inVia confocal Raman microscope (Renishaw) with a 488 nm laser beam. XPS is carried out using HUV System with low energy of 1eV and higher emission of 10 μA.

The mechanical properties were measured using TA instruments DMA Q800 Dynamic Mechanical Thermal Analysis with 0.1%/second strain rate. Thermal conductivities were measured using Quantum Design 14 Tesla Physical Property Measurement System under 300K. Electrical conductivities were measured by Fluke 179 Multimeter.

2.3 Results and discussion

2.3.1 Wet-spinning Process

As presented in 3.1(a), during the wet-spinning process of graphene oxide (GO) fiber under uniaxial flow, the pristine 2 wt. % GO solution changes its particle alignment from gel-like liquid crystals with different orientation ordering (Section I) to the regular alignment of the flowing GO LC dope (Section II), GO LC gel fibers (Section III) and final dried GO fibers (Section IV). Certain volume confinement help GO sheets align paralleled to the needle wall (from Section I to Section

II). The needle has an inner diameter of 0.4 mm, so do the Section III gel-like fiber. After the fiber is air-dried, it has mean diameter (from edge to edge; does not consider voids) of ~50 μm.

CTAB solution is chosen as the coagulation bath due to its positive charge which may play a surprising role in the assembly of the negative-charged GO suspension. This is due to 1) the electrostatic force and 2) the hydrodynamic force. When fibers are being formed, charge neutralization by CTAB, mitigates the dispersion by electrostatic repulsion and helps hydrophobic-hydrophobic interaction to facilitates curling and folding of GO sheets, as illustrated in Figure 3.1(b). After washing, most of the CTAB are removed. It is noted that 1:1 v/v water and ethanol solution is a better solvent to dissolve and wash out CTAB than just pure water.

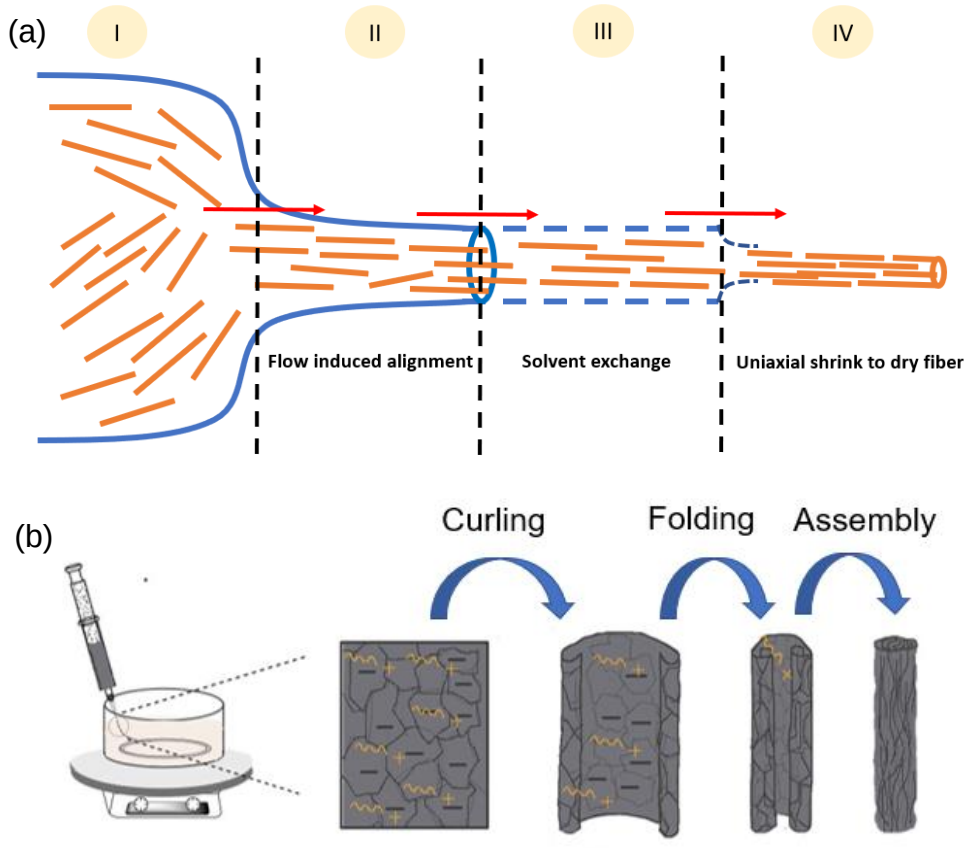

Fig. 2.1. Schematic illustration of (a) structural evolution of the spinning process and (b) the self-assembly of the mechanism of GO fiber.

Generally, greater aspect ratio of building blocks and their better alignment in the fiber axis are the main factors to improve the mechanical performance of polymer and CNT fibers[18,19]. Inspired by this understanding, we employed giant graphene oxide sheets with extremely high aspect ratios as building blocks to reduce defective edges and achieved highly ordered alignment sheets by wet-spinning liquid crystalline gel fibers to make high-performance graphene fibers with both high strength and conductivity. This is the reason why we choose EMD GO as the fiber template because of its large lateral size (~57 μm) (Figure S1).

We choose several temperature points to convert GO to rGO. 400 °C serves the purpose of functional group removal. 1200 °C and 2500 °C are carbonization and graphitization temperature, respectively. In such extreme conditions, the following characterization and discussion prove that the functional groups can be completely removed.

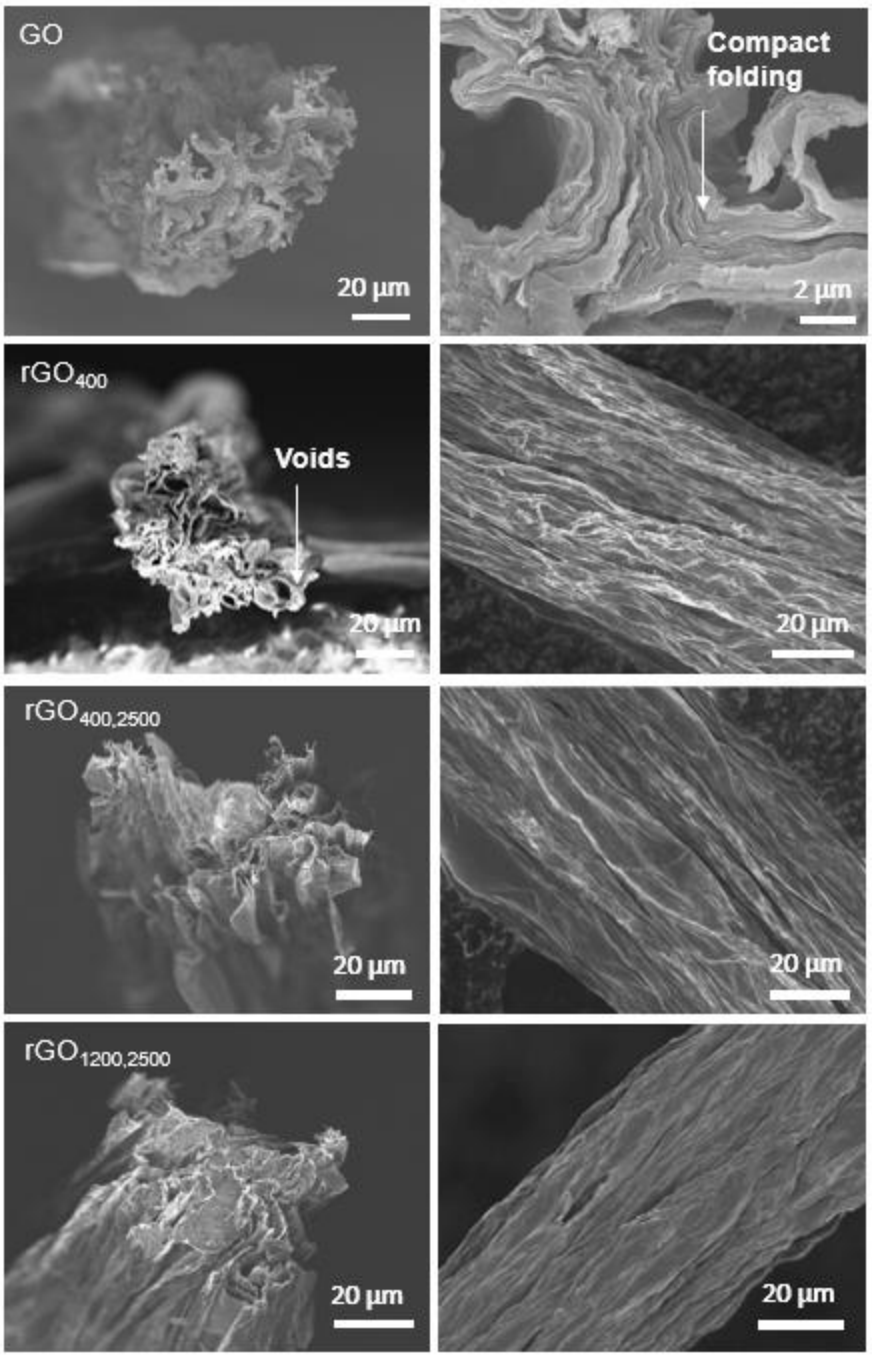

Fig. 2.2. SEM images of GO and rGO fibers for both top-down and cross-sectional views.

To get flat and sharp cross-section surface, the fibers first soaked in ethanol for 15 second and then immersed in liquid nitrogen immediately before getting hard and brittle. Then the fibers were cut by a very sharp scissor. Ethanol filled the holes of the fiber and was solidified in liquid nitrogen. With the support of solidified ethanol, the fibers do not deform during the cutting. As shown in Figure 2.2, GO and rGO fibers exhibit compact folding structure starting from 2-dimensional sheets as seen from its section, and the layered stacking can be identified in the magnified images. Experimental inspections of GO and rGO fibers manifest multiscale defects, which include rough surface with random wrinkles, stacking and voids. When it comes to heat treatment, more inner pores and cavities are found due to functional group cleavage, so the fibers are coarse and loosely packed. The fiber morphology is very different from most of the literatures, which adopt elongational tension force to densify the fibers so that the fibers look compact. Alternatively, we use the batch method to acquire relatively coarse structure as presented in Figure 2.2. without exerting much tensile force on the fibers. By image processing of cross-section SEM photos through ImageJ, the mean cross-sectional area of the fibers is acquired (voids are excluded). GO, rGO_{400}, $rGO_{400,1200}$, and $rGO_{1200,2500}$ are 2581 μm^2, 1158 μm^2, 984 μm^2, and 883 μm^2, respectively. These values are important to calculate conductivities and mechanical strength. In addition, the loosely packed GO also reflected the surprising low density of GO fiber as ~0.25 g/cm^3 measured by us.

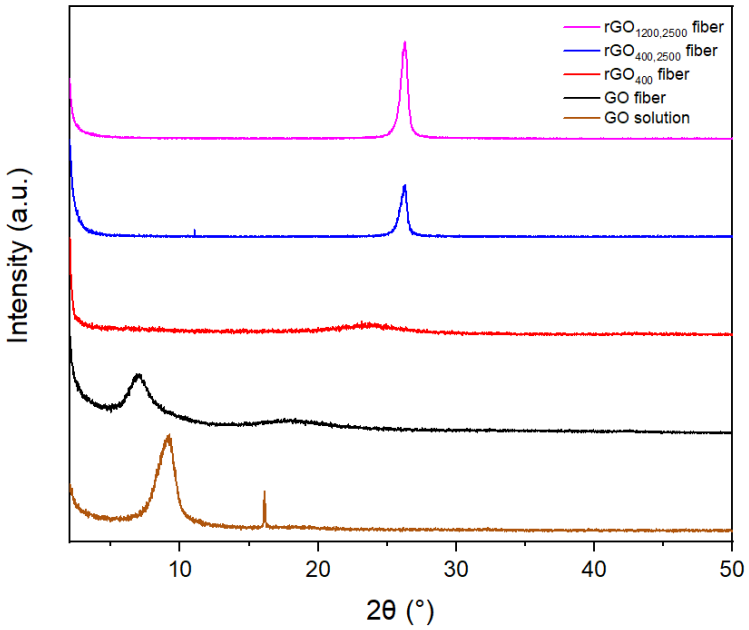

Fig. 2.3. XRD diagrams for EMD GO and rGO fibers. Pristine GO solutions were freeze overnight and then grinded into powders before conducting XRD.

As shown in Figure 2.3, after forming fibers from CTAB coagulation bath, the XRD main peak shifts left with enlarged d-spacings. The increase in d-spacings may come from intercalation of CTAB molecules between GO layers. XRD analysis of the GO fiber annealed at 400 ˚C displayed a significantly different XRD pattern but with a d-spacing (estimated from the maximum peak to be 3.89 Å) close to that of the fully graphitic expanded graphite starting material, which showed a distinct sharp (002) peak at 26.38˚ and a d-spacing that corresponds to 3.38 Å. These results suggest that water and most of the chemical functionalities in the GO sheets are removed after thermal reduction; indicating the effectiveness of the reduction process. The reduction of GO by annealing is further confirmed by the significantly higher electrical conductivity of rGO_{400} fiber (~6.4 x 10^4 S/m) compared to the parent insulating GO fiber. Scherrer equation is adopted to calculate the mean of the crystalline domain of the powdered samples[20]. Number of crystalline layers is

obtained by the quotient of mean size of crystalline domain and d-spacings. It is worth mentioning that the broad rGO_{400} peak between 20° to 26°. This might attribute to the different extent of reduction levels presented in the same bulk sample. $rGO_{400,2500}$ and $rGO_{1200,2500}$ possess sharp peak at 26.38° revealing the typical graphite crystals with identical interlayer spacing as literature[21]. The number of crystalline layers (about a hundred) describes the nature of graphite as well. The removal of functional groups and graphitization facilitates the continuous stacking of graphene sheets into a crystalline structure, as evidenced by the narrowing (002) peak. Meanwhile, the alignment between graphene sheets inside the fiber has been further improved. Interestingly, the number of layers does not change much before and after fiber formation. This tells us an important information that GO does not experience layer restacking and still preserve its initial structure.

	2θ (°)	d-spacing (A°)	FWHM (°)	Crystalline Domain Size (nm)	Number of Layers
GO solution	9.92	8.9	0.74	21.5	24.2
GO fiber	7.04	12.5	1.21	13.2	10.5
rGO_{400} fiber	22.83	3.89	3.89	4.16	10.1
$rGO_{400, 2500}$ fiber	26.30	3.38	0.50	28.1	83.1
$rGO_{1200, 2500}$ fiber	26.28	3.39	0.58	32.6	96.3

Table 2.1. XRD peak analysis for the highest peak (basal plane stackings)

The TGA profile (Figure S2) is another evidence showing that CTAB is not fully removed. For pristine GO solution and GO fiber, oxygen functional groups are removed vigorously at ~190 °C. Interestingly, GO fiber underwent additional 4% weight loss, which is probably the decomposition of CTAB intercalated between GO layers. CTAB decomposition temperature is 240 °C, but it could

be affected by the presence of other functional groups. rGO_{400} has totally 25% of weight loss (at 800 ˚C), meaning that the carbon sheets are still partially oxidized.

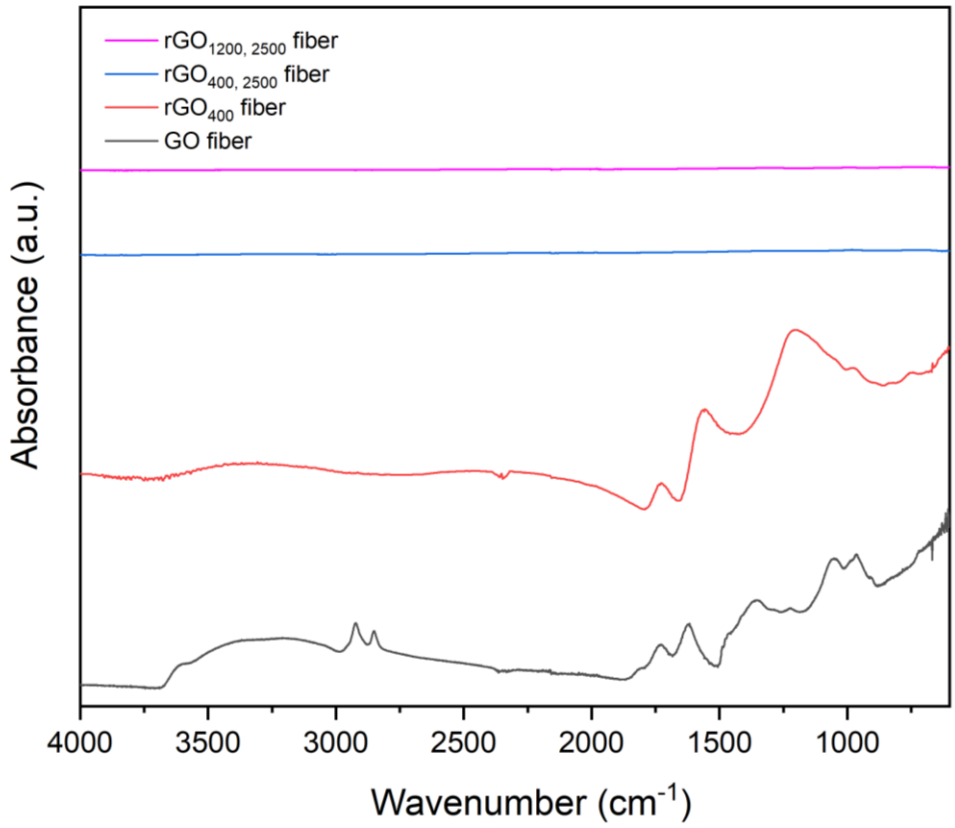

Fig. 2.4. FTIR diagrams for EMD GO and rGO fibers. All the samples were freeze overnight and then grinded into powders before conducting XRD.

As Figure 2.4, the FT-IR spectrum of the as-fabricated GO fiber exhibits a group of bands at 970, 1040, 1622, 1730, 2852, 2924, and 3220 cm^{-1}. The peak at 1040 cm^{-1} denotes the presence of stretching of unoxidized conjugated graphitic domain (C=C). The peak at 1730 and 1622 cm^{-1} arises from the stretching of C=O on carboxyl groups[22]. The two small peaks at 2852 and 2924

cm^{-1} indicates the hydrogen bonded OH groups of dimeric COOH groups and intra-molecular bonded O-H stretching of alcohols respectively[23]. The broad peak at 3220 cm^{-1} indicates the presence of OH stretching in hydroxyl (-OH) and carboxyl (COOH) groups. The curve of rGO_{400} fiber differs from that of GO fiber. The flatter broad peak situated at around 3000-3500 cm^{-1}suggests the presence of much fewer oxygenated functional groups. The disappearance of 2852, 2924 cm^{-1} distinct peaks expresses the decomposition of carboxyl group. The new 1535 cm^{-1} peak shows the of C-C carbon skeletal vibration, which is the evidence of increasing proportion of carbon content. Interestingly, the entirely flat curves of $rGO_{400,2500}$ and $rGO_{1200,2500}$ fibers imply the absence of functional group, i.e. pure graphene/graphite.

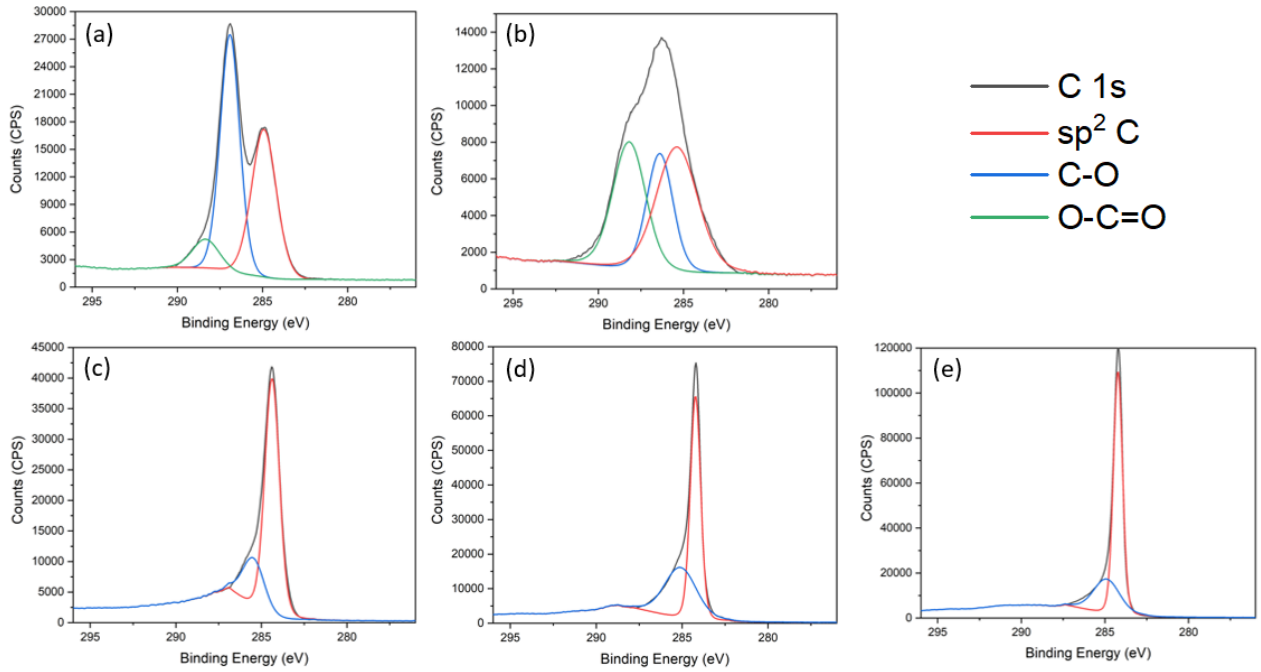

Fig. 2.5. XPS diagrams for (a) pristine EMD GO solution, (b) GO, (c) rGO_{400}, (d) $rGO_{400, 2500}$, and (e) $rGO_{1200, 2500}$ fiber. Only Carbon 1s peak is presented. All the samples were freeze overnight and then grinded into powders before conducting XRD.

Figure 2.5 is the XPS surface characterization of Carbon 1s peaks acquired on GOs before and after thermal annealing. The deconvoluted peaks correspond to contribution of different moieties. The carboxylic C=O bond and hydroxyl C-O groups are presented in (a) and (b), which are typical for pristine GO[24][25]. These peaks disappear (c), (d) and (e), indicating the presence of functional group removal upon thermal treatment. The main remaining peaks are graphitic sp^2 hybridized C=C bond.

Sample	Carbon Content (%)	Oxygen Content (%)
GO solution	64.85	30.90
GO fiber	78.11	21.89
rGO_{400} fiber	89.76	10.24
$rGO_{400, 2500}$ fiber	93.72	6.28
$rGO_{1200, 2500}$ fiber	97.63	2.37

Table 2.2. Raman spectra peak analysis

From Table 2.2, C/O ratio monotonically rises with more intense thermal treatment from 2.1 to 41.2. This is completely reasonable and consistent with the previous FTIR result that high temperature results in functional group cleavage. It is worth noted that for GO solution carbon plus oxygen content is not equal 100, because the pristine gel consists of sulfur, nitrogen, and other

atoms. Interestingly, bromine cannot be detected by XPS. There might be two reasons: (1) CTAB is almost entirely washed out from the rinsing process. (2) CTAB is buried deep inside the layers, not attached on the graphene oxide surface.

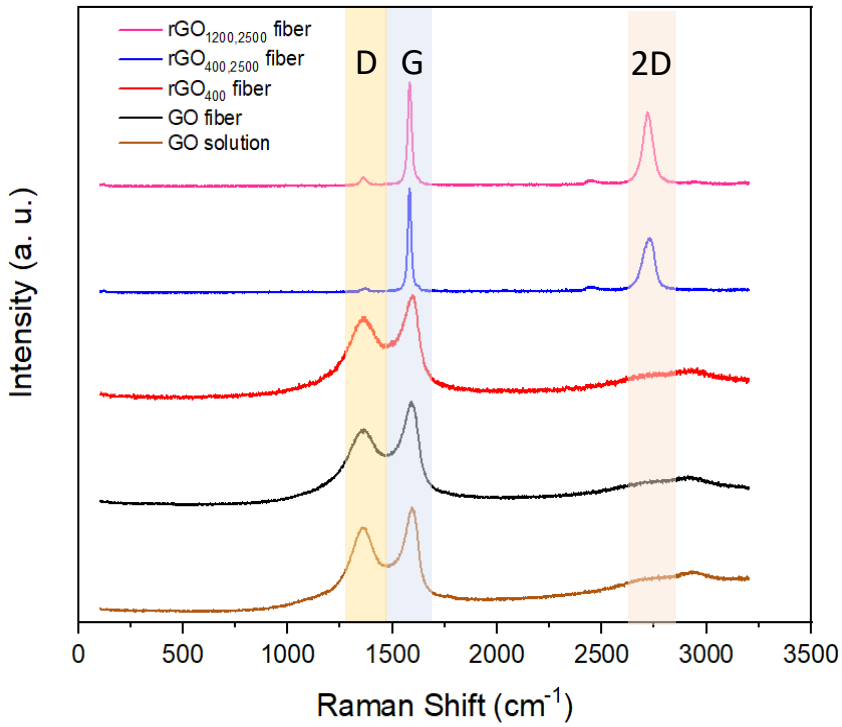

Fig. 2.6. Raman spectra diagram for EMD GO and rGO fibers

Raman spectroscopy can be used as a noninvasive method to characterize graphitic properties such as disorder, edge and grain boundaries, thickness, and exfoliation. As shown in Figure 2.6, energy shift caused by laser excitation creates main peak positions: For GO solution, GO fiber and rGO_{400} fiber: broad D band (1360 cm^{-1}) and G band (1590 cm^{-1}). Functional groups exist on the surface and edge of the planes contribute to the formation of defects and disorders that result in a higher intensity of the D band. The intensity of the D band increases with increasing oxidation. The G band position is due to first-ordered scattering of the E2g mode of vibration and shifts toward

higher wavenumber with an increase in oxidation level. The G band position will reach 1600 cm^{-1} at highest level of oxidation due to the formation of new sp3 carbon atoms in graphitic lattice.

Exposing GO fibers to extreme high temperature environment and the removal of oxygenated functional groups result in structural changes in graphite lattice at the basal plane and at the edges. For $rGO_{400,2500}$ and $rGO_{1200,2500}$: D band (1370 and 1360 cm^{-1}), G band (1581 cm^{-1}) and 2D (2725 and 2720 cm^{-1}) band. The position of G band relates to the number of layers of graphene planes. 1587 cm^{-1}, 1584 cm^{-1}, and 1581 cm^{-1} correspond to single-layer graphene, double-layer graphene or graphite. From our results, $rGO_{400,2500}$ and $rGO_{1200,2500}$ seem to be graphite fibers in terms of the G band position, which is in agreement with previous XRD result. The 2D band is used to evaluate the exfoliation levels. For single layer graphene the 2D band is observed to be a single symmetric peak with a full width at half maximum (FWHM) of ~30 cm^{-1}. Adding successive layers of graphene causes the 2D band to split into several overlapping modes. The I_D/I_G ratio is used to identify oxidation levels. The ratio grows with increasing oxidation levels. The I_D/I_G ratio if rGO_{400} fiber is even higher than GO fiber. This is because after heat treatment, functional groups are removed along with some carbon atoms which are part of original graphene skeleton. It is worth pointing out that for high quality (defect free) single layer graphene, the I_{2D}/I_G ratio will be seen to be equal to 2. Neither of the samples reaches 2.

	I_D/I_G ratio	I_{2D}/I_G ratio	2D FWHM
GO solution	1.21	-	-
GO fiber	1.08	-	-
rGO_{400} fiber	1.28	-	-

$rGO_{400,\ 2500}$ fiber	0.06	1.46	61.4
$rGO_{1200,\ 2500}$ fiber	0.23	1.67	52.9

Table 2.3. Raman spectra peak analysis

2.3.2 Physical Properties

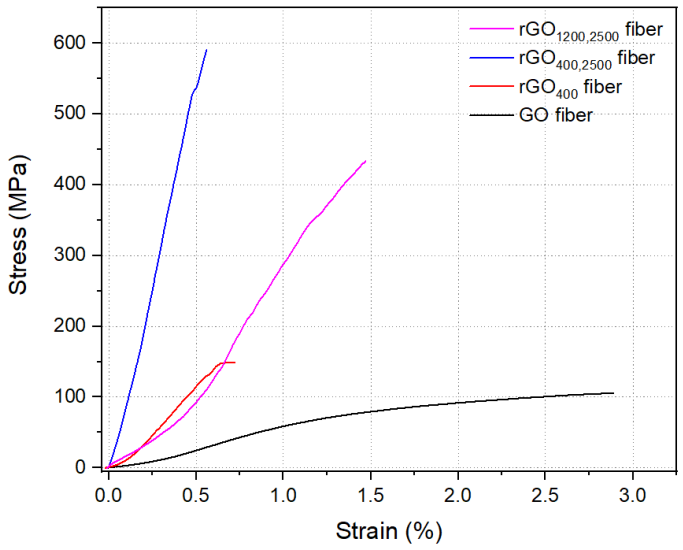

Fig. 2.7. Typical tensile stress curves of GO and rGO fibers.

For mechanical properties measurement, we have measured at least 5 valid sample curves for each sample displaced between two clamps to get standard deviations. Figure 2.7 depicts four curves, which are chosen using the sample with the highest tensile strength for each type of fiber. The deformation mechanism of these GO and rGO fibers can be described by the tension-shear model, a prevalent theory for nanocomposites[26][27][11]. In the neat graphene system, there are three kinds of dominant interactions between graphene sheets, including van der Waals interaction, hydrogen bonds and coordinative cross-linking. In GO fibers, the hydrogen bonds dominate and contribute to their mechanical strength[27]. After chemical reduction, the increasing van der Waals

interaction dominated, along the decreasing interlayer space caused the enhancement in the mechanical properties. Figure 2.7 and Table 2.4 show that tensile strength and Young's modulus enhances for rGO fiber samples. Whereas ultimate elongation drops to 1/3 of GO fiber's value. This denotes the brittleness of rGO fibers that $rGO_{400,\ 2500}$ and $rGO_{1200,\ 2500}$ cannot tolerate strong bending forces.

Sample	Tensile Strength (MPa)	Young's Modulus (GPa)	Maximum Elongation (%)
GO fiber	75.4±25.8	4.1±1.3	2.46±1.1
rGO_{400} fiber	112.8±50.5	37.9±25.5	0.45±0.16
$rGO_{400,\ 2500}$ fiber	322.5±204.7	63.9±27.4	0.57±0.19
$rGO_{1200,\ 2500}$ fiber	273.5±112.0	51.1±24.3	0.60±0.37

Table 2.4. Mechanical properties of the four fibers.

Aside from the CTAB coagulation bath system under room temperature. We chose $CaCl_2$ solutions as the coagulation bath solutions to improve the strength of graphene fibers. Park et al.[28] suggests that the addition of alkaline-earth MCl_2 salts (M equals Mg or Ca) immediately led to agglomeration of the sheets and uncontrollable precipitation, presumably due to the crosslinking of the graphene oxide sheets by the divalent cations. The mechanically strengthened fiber by using divalent cation as bridging agent was also proved by molecular simulation[29]. As presented in Figure 2.8, Ca^{2+}-cross-linked GO fiber has a tensile strength of 101 MPa at 1.01% ultimate elongation. In addition, Paper has shown that higher environmental temperature facilitates graphene oxide restacking[30]. We tried elevating CTAB coagulation bath temperature to 60°C as the fiber formation environment. The resulting GO fiber has a tensile strength of 127 MPa at 1.13%

ultimate elongation. Young's modulus also largely increases to 10.0 and 11.2 GPa, respectively. Although Young's modulus becomes significantly larger with slightly higher tensile strength, the two fibers are much less flexible and more brittle than the reference GO-CTAB fiber made under room temperature. The relatively low maximum elongation has negative effects on fiber fabrication and transportation.

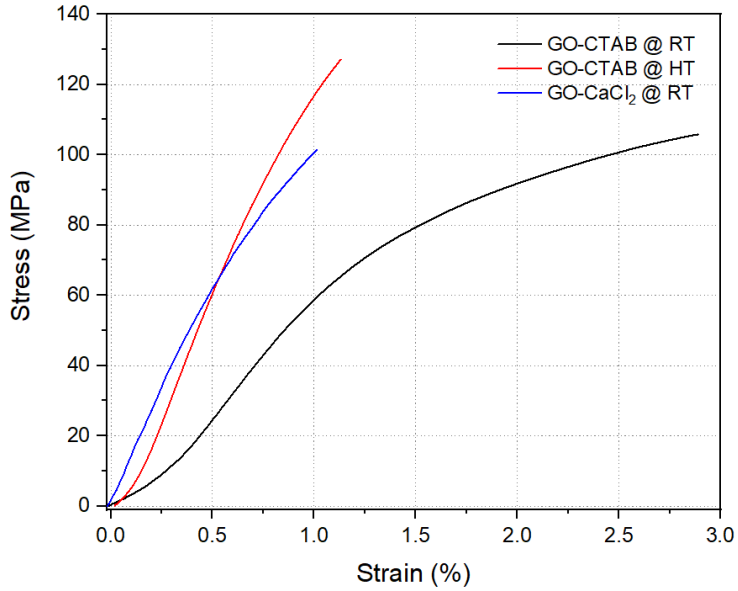

Fig. 2.8. Typical tensile stress curves of GO single fibers. The black curve is the GO-CTAB fiber formed under room temperature of coagulation bath. The red curve is also GO-CTAB fiber but formed under 60°C coagulation bath. The blue curve is GO-$CaCl_2$ fiber formed under room temperature with 2 wt.% of calcium chloride coagulation bath.

Sample	Thermal Conductivity (W/K-m)	Electrical Conductivity (S/m)
GO fiber	57	Non-conductive

rGO_{400} fiber	301	6.44×10^4
$rGO_{400, 2500}$ fiber	1,657	1.77×10^5
$rGO_{1200, 2500}$ fiber	992	1.33×10^5

Table 2.5. Electrical and thermal conductivities of GO and rGO fibers.

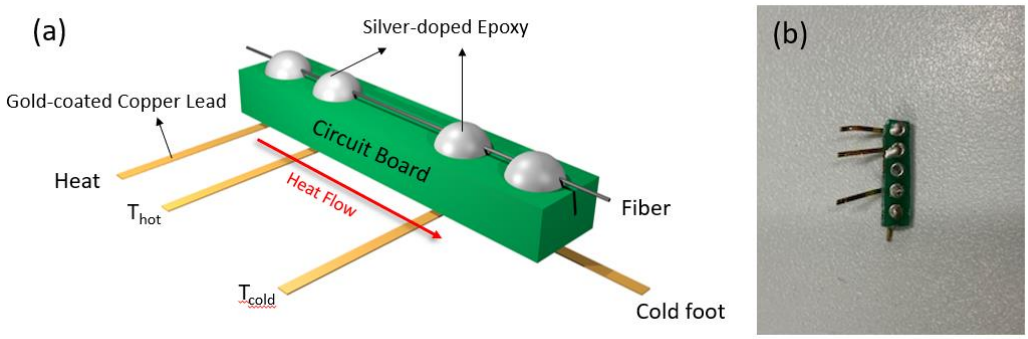

Fig. 2.9. (a) Scheme and (b) picture of a sample prepared for electrical and thermal conductivities measurements. Heat square waves flow through the end leads and the middle two leads measure the temperature differences.

After thermal reduction, based on the highly-aligned sp^2 graphene/graphite sheets, the rGO fibers shows excellent electrical and thermal conductivity, of 1.3-1.7 $\times$ 10^5 S/m, about 20 times higher than that of reduced graphene papers (7.2 $\times$ 10^3 S/m)[31] and about 5 times higher than that of graphene fibers assembled from small graphene sheets (2.5 $\times$ 10^4 S/m)[32], because of the giant size of rGO sheets which reduce the proportion of edges and defects and their regular alignment in the fibers. This is a strong evidence of "complete" cleavage of oxygenized functional groups. To investigate the electrical resistance of rGO fibers, the fibers were mounted on an insulating circuit board by silver-doped conducting epoxy and each fiber sample connected to four copper

leads (Figure 2.9). The resistivity was operated manually by multimeter by touching two different leads. The resistance is proportional to the length of the fiber, which shows the reliability of this method. The extremely high conductivity of the rGO fibers together with their lightness makes them useful as flexible and lightweight cables in wearable electronic devices.

We measure the thermal conductivity by PPMS system. The temperature was set permanently at 300K, using the same fiber mounting method as electrical conductivity measurement. This is standard four-point probe method as shown in Figure 2.8, and we put the sample in an insulated chamber to ensure the accuracy. It is known that the thermal conductivity of multilayer graphene is reduced in comparison to single-layer graphene, due to interlayer interactions and vibrational restrictions from neighboring layers, which limits the free vibration of the graphene sheets and imposes resistance on phonon transport[33]. In addition, we believe that the thermal transport properties of our rGO fibers are not an indication of the in-plane thermal conductivity of the individual layers due to the tangled nature of the rGO sheets in the fiber and lattice defects that are introduced during GO sheet synthesis and subsequent reduction processes. Even for the highest result (1657 W/m-K), however, the value is much lower than the theoretical value of single layer graphene (up to 5300 W/m-K), which is attribute to the defect edges.

The electrical and thermal conductivity results are very precious that we have proved that even relatively coarse fibers with a lot of inner pores and voids, high conductivities can still be achieved as long as the initial graphene oxide building block is large enough.

It is pertinent to mention that the result is consistent with the I_D/I_G ratio in Table 2.3. For rGO fibers, the lower I_D/I_G ratio, which indicates lower amount of defect, results in higher conductivities. The trend is identical for both electrical and thermal conductivity that $rGO_{400, 2500} > rGO_{1200, 2500} > rGO_{400} >$ GO fibers. Interestingly, GO fiber is electrically insulated but possesses very high thermal conductivity (57 W/m-K) which is comparable to many metals such as nickel (91 W/m-K) and iron (80 W/m-K). This unique property may have a few potential applications.

2.4. Conclusion

In conclusion, we designed and fabricated graphene oxide and graphite fibers start with GO sheets by wet spinning. The large size of the constituent graphene sheets together with their good alignment resulted in a considerable improvement in the mechanical performance of the graphene fibers. Surprisingly, the coarse graphite fibers possessed a tensile strength up to 0.6 GPa among neat graphene materials (or high specific strength based on carbon's low density), with extraordinary electrical and thermal conductivities which are comparable to theoretical value of graphene. Such multifunctional graphene fibers have promise in versatile applications such as functional textiles, flexible and wearable sensors, and supercapacitors devices. The realization of strong fibers composed of large graphene sheets opens the door for the next-generation of high-performance fibers with superb strength, excellent toughness, and rich functionalities fabricated by a room-temperature supramolecular assembly strategy.

Acknowledgment

This work was funded by KISCO Co. in South Korea. The graphene oxide material was provided by EMD Material Performance Co. All the material characterizations were obtained via facilities

at the Cornell Center for Materials Research. I also want to thank all the staffs in CCMR for their kind and knowledgeable help.

REFERENCES

[1] K.S. Geim, A. K. and Novoselov, The rise of graphene, Nat. Mater. 6 (2007) 183–191.

[2] R. Raccichini, S.P. and B.S. , Alberto Varzi, energy storage, Nat. Mater. 14 (2015) 271–279. doi:10.1038/NMAT4170.

[3] L. Tao, K. Zhang, H. Tian, Y. Liu, D. Wang, Y. Chen, Y. Yang, T. Ren, Graphene-Paper Pressure Sensor for Detecting Human Motions, ACS Nano. 11 (2017) 8790–8795. doi:10.1021/acsnano.7b02826.

[4] W. Li, X. Geng, Y. Guo, J. Rong, Y. Gong, L. Wu, X. Zhang, P. Li, Reduced Graphene Oxide Electrically Contacted Graphene Sensor for Highly Sensitive Nitric Oxide Detection, ACS Nano. 5 (2011) 6955–6961. doi:10.1021/nn201433r.

[5] Y. Li, H. Wang, L. Xie, Y. Liang, G. Hong, H. Dai, MoS2 Nanoparticles Grown on Graphene: An Advanced Catalyst for the Hydrogen Evolution Reaction, J. Am. Chem. Sociaty. 133 (2011) 7296–7299. doi:10.1021/ja201269b.

[6] H. Wang, T. Maiyalagan, X. Wang, Review on Recent Progress in Nitrogen-Doped Graphene : Synthesis , Characterization , and Its Potential Applications, ACS Catal. 2 (2012) 781–794. doi:10.1021/cs200652y.

[7] Z. Xu, C. Gao, Aqueous Liquid Crystals of Graphene Oxide, ACS Nano. (2011) 2908–2915. doi:10.1021/nn200069w.

[8] T.H. Han, S. Ouk, Graphene oxide liquid crystals: a frontier 2D soft material for graphene-based functional materials, Chem. Soc. Rev. 47 (2018) 6001–6446. doi:10.1039/c8cs00299a.

[9] H.P. Cong, X.C. Ren, P. Wang, S.H. Yu, Wet-spinning assembly of continuous, neat, and macroscopic graphene fibers, Sci. Rep. 2 (2012) 1–6. doi:10.1038/srep00613.

[10] R. Jalili, S.H. Aboutalebi, D. Esrafilzadeh, R.L. Shepherd, J. Chen, S. Aminorroaya-Yamini, K. Konstantinov, A.I. Minett, J.M. Razal, G.G. Wallace, Scalable one-step wet-spinning of graphene fibers and yarns from liquid crystalline dispersions of graphene oxide: Towards multifunctional textiles, Adv. Funct. Mater. 23 (2013) 5345–5354. doi:10.1002/adfm.201300765.

[11] Z. Xu, H. Sun, X. Zhao, C. Gao, Ultrastrong fibers assembled from giant graphene oxide sheets, Adv. Mater. 25 (2013) 188–193. doi:10.1002/adma.201203448.

[12] G. Xin, T. Yao, H. Sun, S.M. Scott, D. Shao, G. Wang, J. Lian, Highly thermally conductive and mechanically strong graphene fibers, Science (80-.). 349 (2015) 1083–1088.

[13] Z. Dong, C. Jiang, H. Cheng, Y. Zhao, G. Shi, L. Jiang, L. Qu, Facile fabrication of light, flexible and multifunctional graphene fibers, Adv. Mater. 24 (2012) 1856–1861. doi:10.1002/adma.201200170.

[14] M.K. Shin, B. Lee, S.H. Kim, J.A. Lee, G.M. Spinks, S. Gambhir, G.G. Wallace, M.E. Kozlov, R.H. Baughman, S.J. Kim, Synergistic toughening of composite fibres by self-alignment of reduced graphene oxide and carbon nanotubes, Nat. Commun. 3 (2012) 650–

658. doi:10.1038/ncomms1661.

[15] X. Zhang, X. Fan, C. Yan, H. Li, Y. Zhu, X. Li, L. Yu, Interfacial microstructure and properties of carbon fiber composites modified with graphene oxide, ACS Appl. Mater. Interfaces. 4 (2012) 1543–1552. doi:10.1021/am201757v.

[16] S. Wang, N. Liu, J. Su, L. Li, F. Long, Z. Zou, X. Jiang, Y. Gao, Highly Stretchable and Self-Healable Supercapacitor with Reduced Graphene Oxide Based Fiber Springs, ACS Nano. 11 (2017) 2006–2074. doi:10.1021/acsnano.6b08262.

[17] Z. Li, Z. Xu, Y. Liu, R. Wang, C. Gao, Multifunctional non-woven fabrics of interfused graphene fibres, Nat. Commun. 7 (2016) 1–11. doi:10.1038/ncomms13684.

[18] K. Koziol, High-Performance Carbon Nanotube Fiber Krzysztof Koziol, Science (80-.). 1892 (2008) 1892–1896. doi:10.1126/science.1147635.

[19] H.G. Chae, S. Kumar, Making Strong Fibers, Science (80-.). 319 (2008) 908–909. doi:10.1126/science.1153911.

[20] D.R. Chowdhury, C.S. and A. Paul, Role of graphite precursor and sodium nitrate in graphite oxide synthesis, RSC Adv. 4 (2014) 15138–15145. doi:10.1039/c4ra01019a.

[21] P.L. De Andres, R. Ramírez, J.A. Vergés, Strong covalent bonding between two graphene layers, Phys. Rev. B. 77 (2008) 1–5. doi:10.1103/PhysRevB.77.045403.

[22] T. Rattana, S. Chaiyakun, N. Witit-anun, N. Nuntawong, P. Chindaudom, Preparation and characterization of graphene oxide nanosheets, Procedia Eng. 32 (2012) 759–764. doi:10.1016/j.proeng.2012.02.009.

[23] K. Josepovits, Y. Sanakis, D. Petridis, I. De, Evolution of Surface Functional Groups in a Series of Progressively Oxidized Graphite Oxides, Chem. Mater. (2006) 2740–2749.

[24] F. Perrozzi, S. Prezioso, L. Ottaviano, Graphene oxide: From fundamentals to applications, J. Phys. Condens. Matter. 27 (2015) 013002. doi:10.1088/0953-8984/27/1/013002.

[25] F.T. Johra, J.W. Lee, W.G. Jung, Facile and safe graphene preparation on solution based platform, J. Ind. Eng. Chem. 20 (2014) 2883–2887. doi:10.1016/j.jiec.2013.11.022.

[26] P. Miaudet, S. Badaire, M. Maugey, A. Derre, Hot-Drawing of Single and Multiwall Carbon Nanotube Fibers for High Toughness and Alignment, Nano Lett. 5 (2005) 2212–2215. doi:10.1021/nl051419w.

[27] J.P. Rourke, P.A. Pandey, J.J. Moore, M. Bates, I.A. Kinloch, R.J. Young, N.R. Wilson, The Real Graphene Oxide Revealed : Stripping the Oxidative Debris from the Graphene-like Sheets **, Angew. Chemie Int. Ed. 50 (2011) 3173–3177. doi:10.1002/anie.201007520.

[28] D. Ions, E. Mechanical, S. Park, K. Lee, G. Bozoklu, W. Cai, Ḱ.S.T. Nguyen, R.S. Ruoff, Graphene Oxide Papers Modified by Divalent Ions-Enhancing_ Mechanical Properties via Chemical Cross-Linking_Supporting_ Information.pdf, ACS Nano. 2 (2008) 572–578.

[29] E. Gao, Y. Cao, Y. Liu, Z. Xu, Optimizing Interfacial Cross-Linking in Graphene-Derived Materials, Which Balances Intralayer and Interlayer Load Transfer, ACS Appl. Mater.

Interfaces. 9 (2017) 24830–24839. doi:10.1021/acsami.7b04411.

[30] Y. Niu, Q. Fang, X. Zhang, P. Zhang, Y. Li, Reduction and structural evolution of graphene oxide sheets under hydrothermal treatment, Phys. Lett. A. 380 (2016) 3128–3132. doi:10.1016/j.physleta.2016.07.027.

[31] Z. An, O.C. Compton, K.W. Putz, L.C. Brinson, S.T. Nguyen, Bio-inspired borate cross-linking in ultra-stiff graphene oxide thin films, Adv. Mater. 23 (2011) 3842–3846. doi:10.1002/adma.201101544.

[32] Z. Xu, C. Gao, Graphene chiral liquid crystals and macroscopic assembled fibres, Nat. Commun. 2 (2011) 571–579. doi:10.1038/ncomms1583.

[33] Z. Wei, Z. Ni, K. Bi, M. Chen, Y. Chen, In-plane lattice thermal conductivities of multilayer graphene films, Carbon N. Y. 49 (2011) 2653–2658. doi:10.1016/j.carbon.2011.02.051.

APPENDICES

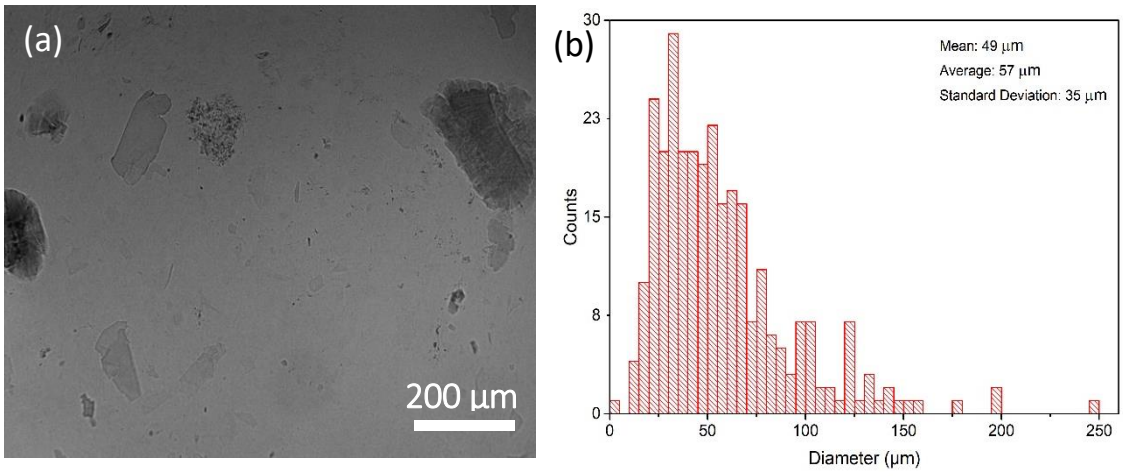

Fig. S1. (a) Optical microscope image and (b) lateral size distribution of pristine EMD GO gel solution.

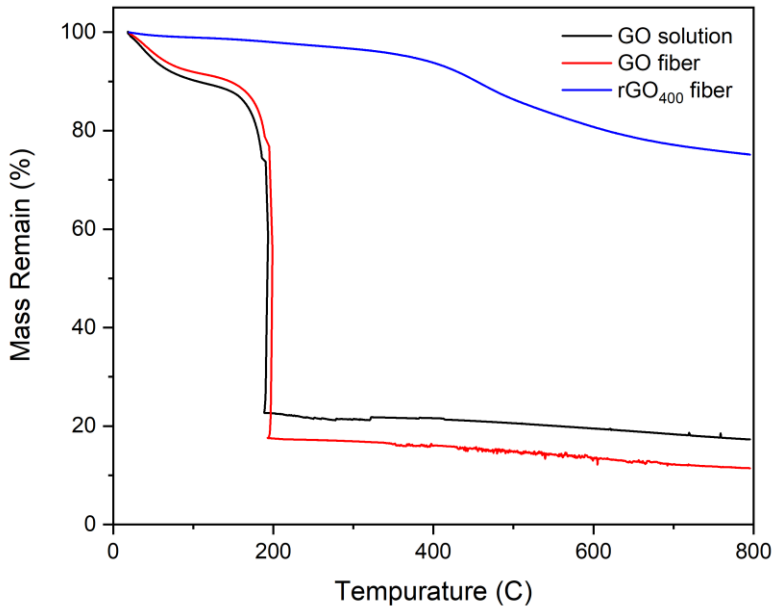

Fig. S2. Thermogravimetric analysis (TGA) diagram for pristine EMD GO solution, GO fiber, and rGO_{400} fiber from room temperature to 800°C. The ramp rate is 10°C/min.

CHAPTER 3

Graphene Oxide Fiber Water Re-dispersion for Enhanced Transportation Efficiency

3.1 Introduction

As graphene is expensive and relatively hard to produce, great efforts are made to find effective yet inexpensive ways to make and use graphene derivatives or related materials. Graphene oxide (GO) is one of those materials - it is a single- or several-atomic layered carbonaceous material, made by the powerful oxidation of graphite[1], which is cheap and abundant in nature. GO is an oxidized form of graphene with abundant oxygen-containing groups. Among many advantages of GO, the lower cost of its manufacturing in comparison to graphene is one of the major ones. Moreover, GO can practically be deposited on any substrate and then be converted to the conductive graphene[2,3]. For this specific reason, GO is used in the production of transparent conductive films applicable in flexible electronics[4], chemical sensors[5], etc. Some other applications include chemical catalysis[6,7] and water and wastewater treatments[8,9]. Due to its high surface area, GO is also used as electrode materials in batteries[10,11], capacitors[12,13] and solar cells.

However, GO has some obvious drawbacks. Firstly, it is usually produced and transported in the form of dilute dispersion in water. We all know that graphene oxide was commonly prepared using a modified Hummers' method[1][14], which use massive water as solvent. This will increase the mass of materials to be transferred by a factor of hundred or even thousand. In the shipment of a 5 kg GO, as an example, one should deal with transporting a 500 liter of liquid. Such a huge volume to be transferred seems to have a lot of technical difficulties and will generate a cost of redundancy.

Secondly, due to the toxicity of GO, there have been increasing concerns over its incidental and accidental release into the environment and the living system[15][16]. Therefore, transportation of graphene oxide other than solution form is an urgent concern for industry.

We proposed a novel self-assembled graphene oxide fiber to solve the problem mentioned above. This method implements wet spinning process to extract GO particles, which is cheap, fast, and easy to scale up[17]. By adding a slight amount of coagulation agent, compact fibers or platelets form immediately soon after extruding pristine gel solution. If graphene oxide can be transported in fiber form, the largely reduced volume will dramatically bring down the cost. Fiber is also much easier to manage than gel solution, and this could further prevent graphene oxide from leaking to environment and harm living organisms. The only concern is whether these fibers can be re-dispersed back into water and remain the chemical and physical properties, and whether the water solution retains important liquid crystallinity. As a result, in this chapter, we investigate the properties of the fiber redispersion solution.

3.2 Experimental Methods

3.2.1 Materials

Graphene oxide aqueous solution was purchased from EMD Performance Materials Corp. and Kisco Co. Hexadecyltrimethylammonium bromide (CTAB) (>98%) was purchased from Sigma-Aldrich. Sodium hydroxide pellet bottle was purchased from Mallinkrodt Chemicals. Ethyl alcohol (>99%) was purchased from VWR Chemicals.

3.2.2 Graphene Oxide Fiber Fabrication

2 wt.% of degassed GO dispersion in water was sonicated for 30 minutes and then loaded in a plastic syringe and injected into a rotating CTAB coagulation bath (15 rpm) with the infusion rate of 0.6 ml/min. The coagulation bath consisted of 1:1 volume ratio of water and ethanol, and CTAB concentration is 0.5 mg/ml. The obtained fibers remained in the bath for 30 min before winding around a Teflon bar, and then soaked the bar in a washing bath (1:1 volume ratio of water and ethanol) for another 60 min. The fibers then were unwounded from the Teflon bar and dried at room temperature after taking out from the bath.

NaOH coagulation bath was made in the same way as CTAB's, with identical coagulation bath concentration of 1 mg/ml. GO solution was casted into the coagulation bath for 10 min and 30 min, respectively. The rest steps were the same as CTAB's.

3.2.3 Water Redispersion

The fibers are grinded into powder using a mortar and pestle. The powdered GO were then dispersed in water (1 wt.%) by 30 seconds of vortex mixer and 3 hours of sonication bath. GO-CTAB samples underwent 3 minutes of further ultra-sonication.

3.2.4 pH Titration

10 wt.% sodium hydroxide aqueous solution was used for rapid pH adjustment to titrate pristine Kisco 40 GO gel solution. 1 wt.% sodium hydroxide dilute solution for precise control. The solution was adjusted to pH=11. The pH titration is for the purpose of zeta-potential measurement.

3.2.5 Characterization Methods

X-ray diffraction (XRD) patterns were determined by a D8 Advance ECO powder diffractometer (Bruker Corporation) using a high-brilliance 1 kW X-ray source. The Fourier transformed infrared

(FTIR) spectrum was measured with a PerkinElmer Frontier MIR Spectrometer coupled with a $LiTaO_3$ MIR detector in the range of 600−4000 cm^{-1} with 32 scans for each sample. Optical Microscope (OM) was utilized by an Amscope 40-1000X binocular compound microscope with digital camera. Zeta potentials were obtained by Zetasizer Nano ZS, Malvern. Polarized Optical Microscope (POM) was conducted using Olympus BX51 with cross polarization filter with a rotating stage. All the GO gel samples were loaded in capillary tubes with inner diameter of 0.5 mm. Small angle X-ray diffraction (SAXS) patterns were determined by an Anton Paar SAXess mc^2. The X-ray exposure time is 5 minutes. The X-ray source is a long-fine focus (LLF) sealed copper tube with line and pint focus (40 kV/50 mA, l = 0.1542 nm).

3.3 Results and Discussion

3.3.1 Conformation and Characterization

We use two different graphene oxide sources: 2 wt.% graphene oxide gel solution provided by EMD Performance Material Co. and by KISCO Co. The main difference of the two different GO is the lateral size.

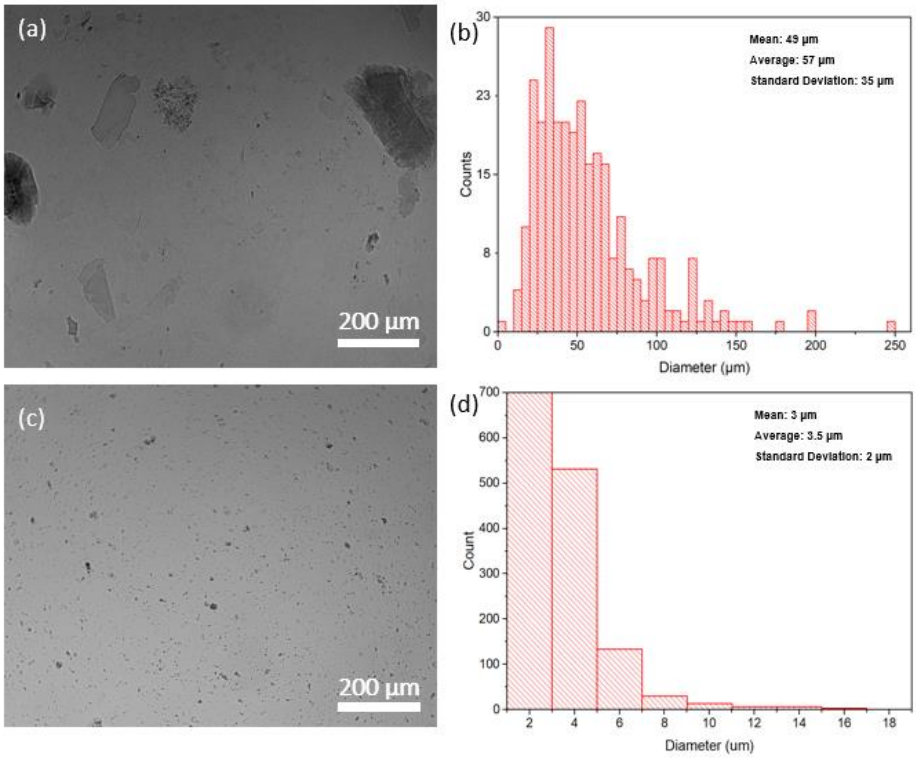

Fig. 3.1. (a) Optical microscope images of LGO pristine gel solution and (b) particle lateral size distributions. (c) Optical microscope images of SGO pristine gel solution and (d) particle lateral size distributions.

We choose GO provided from two different companies: EMD Performance Materials and Kisco Corporation (Figure 3.1). Both are well dispersed in water solution and possess a similar degree of oxidization. GO provided by EMD has average lateral size of 57 µm, which is 10 times larger than that provided by Kisco. So EMD GO is named as large GO (LGO), and Kisco GO is called small GO (SGO). The purpose of using two different GO templates is to show the influence of sheet size. We introduced CTAB as coagulation agent to efficiently transform GO gel solution to solid fibers by wet spinning. The fibers then re-dispersed back into water to obtain GO-CTAB

solution and conducted chemical and physical properties characterization or analysis. We will use "GO-coagulant" as the names of fiber redispersion samples.

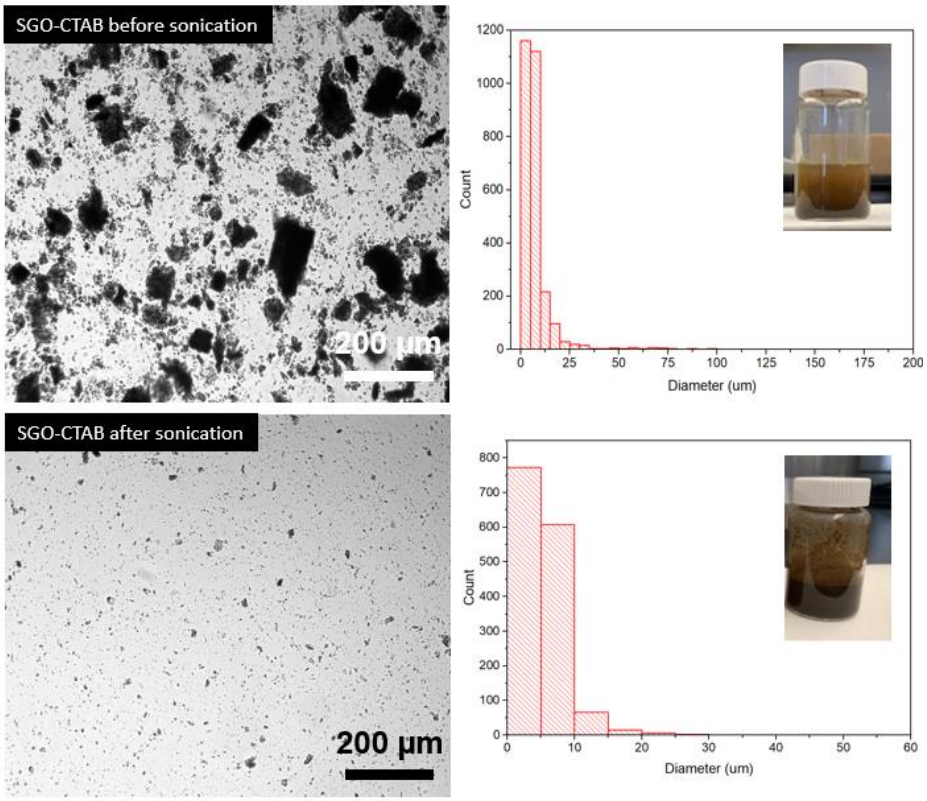

Fig. 3.2. From left to right: Optical microscope images of SGO-CTAB fiber water dispersion, particle lateral size distributions, and 2 wt.% SGO-CTAB water solution images. The top and bottom are solution suspension before and after sonication and ultra-sonication.

Figure 3.2 showed the image of the re-dispersed SGO-CTAB fiber solution. Ultra-sonication drastically facilitated the dispersion of GO and decrease the lateral size of the GO sheets. Before sonication, the large agglomerates precipitated within 5 minutes. Color gradient is easily seen. After ultra-sonication for 3 minutes, the slurry was well dispersed in water even after resting a day. Yet, the sonicated particles still look opaque. Why this happens?

Although GO sheets are highly dispersed in the GO solution, interestingly, even after the GO solution is dried, water molecules remain stuck in the GO powder via hydrogen bonding interactions between water molecules and oxygen-containing functional groups of GO, and these water molecules are often referred to as “intercalated” water molecules[18,19]. The intercalated water molecules play a decisive role in the restacking of the GO because the hydrogen bonding facilitates interactions between GO sheets, resulting in aligning the GO sheets in the same orientation. Herein, from the optical microscope images, the particles reveal black even after ultra-sonication. We assume that CTAB is a strong coagulation agent which helps GO sheets aggregate. Hydrogen bonding interactions and acidic environment facilitate GO sticking together. That is, the introduction of CTAB and water molecules is not ideal for returning GO fibers back to initial gel states.

As a result, a weaker coagulant/better dispersant is needed to reduce GO’s strong tendency to agglomerate, but this chemical cannot be too weak to make GO form fiber. Triton X-100 and sodium cholate are two well-known surfactants, but unlike CTAB, they cannot even form fibers and will decompose within a few minutes in the bath (S1). Therefore, a coagulant which lay in between may be a better option. Literature states that sodium and potassium hydroxide are weaker coagulant than alkaline earth salts[17][20]. This is an important clue that maybe, for example, sodium hydroxide works better in order to preserve graphene oxide conformation and even the liquid crystallinity of its gel solution.

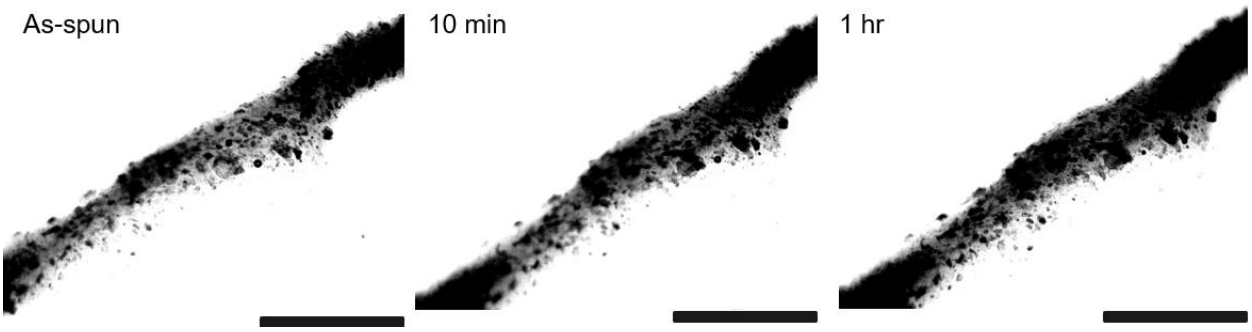

Fig. 3.3. Optical microscope images of LGO gel-like fiber in 1 wt.% NaOH coagulation bath. The scale bar is 500 μm.

Each GO sheet is negatively charged when dispersed in aqueous solution due to the ionization/hydrolysis of O-groups and GO zeta-potential can reach ζ = -60 mV at pH 10 (Figure 3.5). The stability of aqueous GO colloids was therefore attributed to electrostatic repulsion rather than hydrophilic interaction. But why sodium hydroxide can be used as a coagulation agent? Addition of NaOH solution causes GO to precipitate from solution, due to salting-out effects. GO extracted from high pH solution and dried collapsed into star-like formation comprising several sheets or bundles[21].

Figure 3.3 shows the image of the LGO fiber in NaOH coagulation bath. There is almost no conformational change within the graphene oxide sheets when the fibers formed in the NaOH bath even after 1 hour of soaking time. But when it comes to the water re-dispersion solution from dried LGO-NaOH fibers, different soaking time resulted in different conformation. Figure 3.4 (a) and (b) showed flat and more transparent sheet; yet (c) and (d) revealed striped and distorted flakes. Less soaking time (i.e. 10 min) preserved the sheet conformation; that is, become less affected by the presence of NaOH. The conformation variation directly affected liquid viscosity. Lesser surface interaction between sheets resulted in lower viscosity if the sheets are more distorted.

Fortunately, Figure 3.4 (a) and (b) manifest more complete and exfoliated sheets compared to Figure 3.3. We draw a conclusion that sodium hydroxide is a better coagulant on preserving GO conformation. This is also proved by the morphology of the electrosprayed GO particles shown in S3.

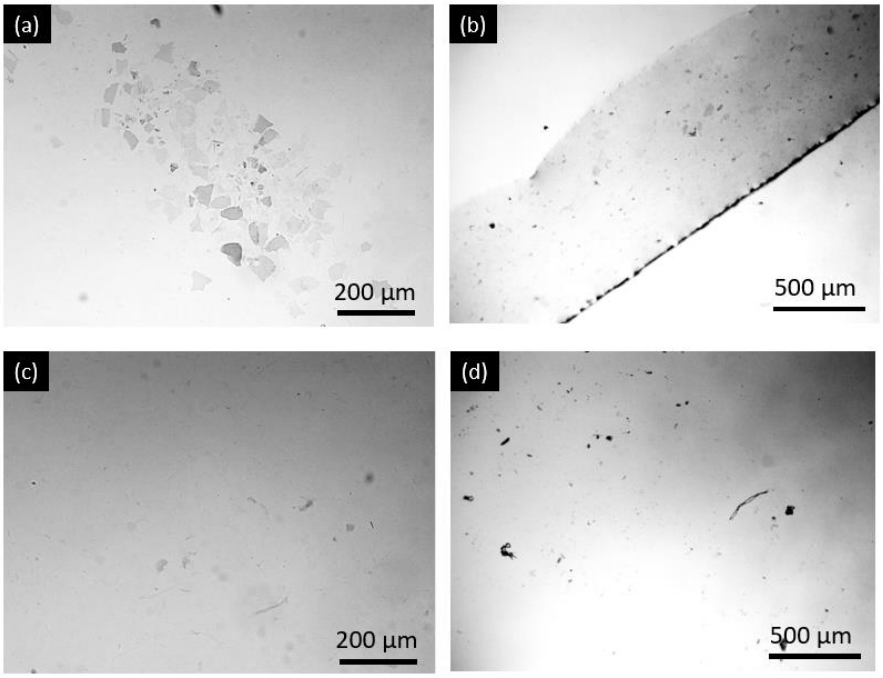

Fig. 3.4. Optical microscope images of water re-dispersion of LGO fiber. The gel fibers were immersed in 1 wt.% NaOH coagulation bath for a) b) 10 minute and c) d) 30 minute.

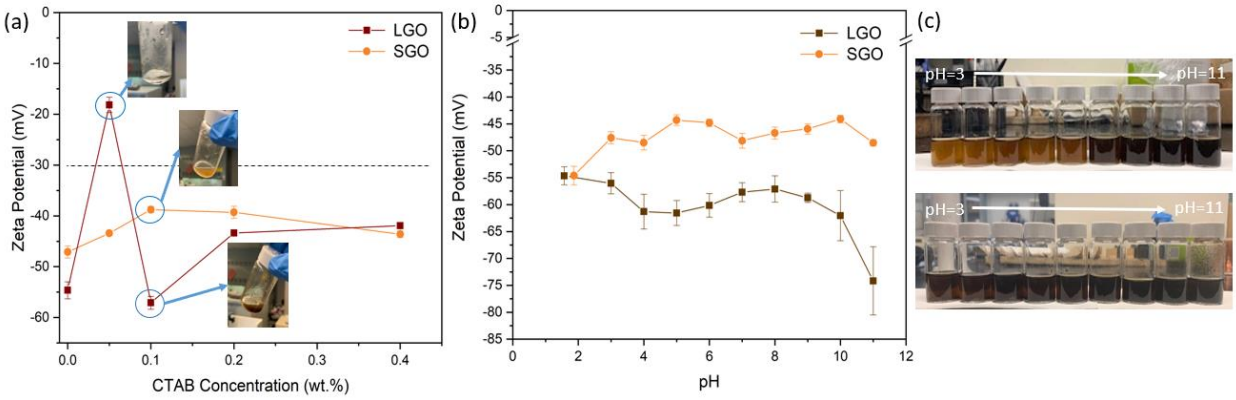

Fig. 3.5. Zeta potentials for (a) LGO and SGO versus different CTAB coagulation bath concentration and (b) LGO and SGO versus different pH value. NaOH was used for titration. (c) The photo shows LGO and SGO solutions after pH adjustment. The solution concentration is less than 1 wt.% adjustment to show color differences.

Figure 3.5 (a) presents the relationship between zeta potential and concentration of CTAB. The 0.0 wt.% point is the pristine GO gel solution and the rest four points are GO fiber re-dispersion with different coagulant concentration. It is well-known that GO can form well-dispersed aqueous colloids. Our study on the surface charge (zeta potential) of as-prepared GO sheets shows that these sheets are highly negatively charged when dispersed in water (Figure 3.5). Apparently, this is a consequence of ionization of the carboxylic acid and phenolic hydroxyl groups that are known to exist on the GO sheet. This result suggests that the formation of stable GO colloids should be attributed to electrostatic repulsion, rather than just the hydrophilicity of GO. It is known that the residual electrolytes can neutralize the charges on the sheets, destabilizing the resulting dispersions[10]. However, even under the presence of coagulant CTAB, zeta potential just slightly becomes less negative (ζ= ~-40). It is denoted that zeta potential values more negative than –30 mV are generally considered to represent sufficient mutual repulsion to ensure the stability of a dispersion, as is well known from colloidal science[22]. Thus, the stability of re-dispersed GO-CTAB solution is approved. Figure 3.5 (b) indicates the relationship between zeta potential and different pH value. The pH = 1.87 (SGO) and pH = 1.57 (SGO) points represent the pristine GO gel solutions and the rest points are pH-adjusted solutions. Unlike what the literature has shown[10], there is no distinct trend between zeta potentials and pH values. Huge negative values

of pristine LGO and SGO solution might come from sulfuric acid residue by Hummers' method. The picture in Figure 3.5 (c) reveals the gradual color changes from brown to black especially from pH=7 to 8 for SGO. LGO does not exhibit dramatic color change, but gradually darkened color is still observed.

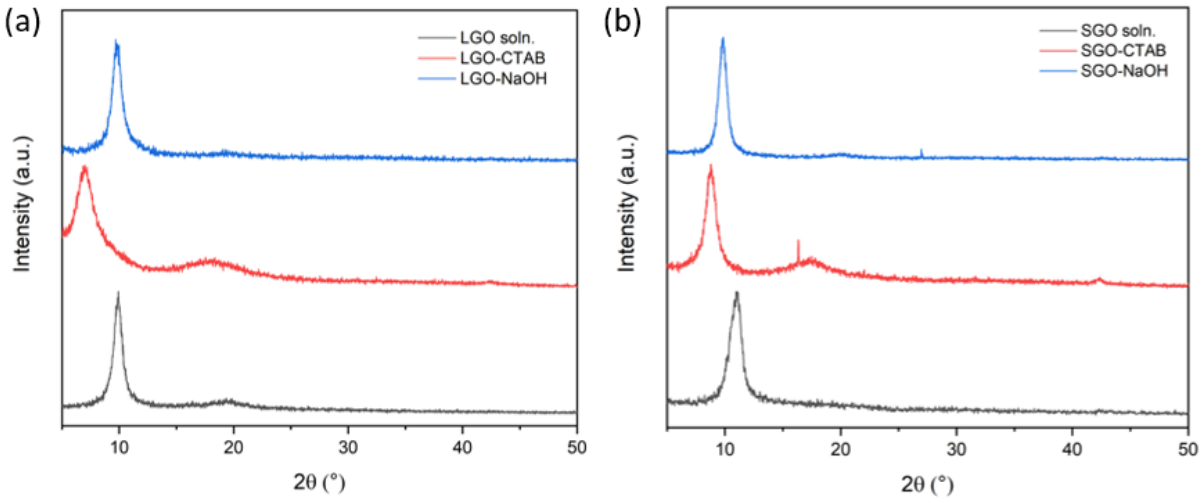

Fig. 3.6. XRD diagrams for (a) LGO and (b) SGO pristine solution and fibers using different coagulation bath. Pristine GO solutions were freeze overnight and then grinded into powders before conducting XRD.

	2θ (°)	d-spacing (A°)	FWHM (°)	Crystalline Domain Size (nm)	Number of Layers
SGO	11.10	7.96	1.13	14.12	17.74
SGO-CTAB	8.79	10.05	1.02	15.62	15.54
SGO-NaOH	9.84	8.98	0.78	20.44	22.76
LGO	9.92	8.91	0.74	21.54	24.19
LGO-CTAB	7.04	12.54	1.21	13.15	10.49
LGO-NaOH	9.68	9.13	0.85	18.75	20.55

Table 3.1. XRD peak analysis for the highest peak (basal plane stackings)

Figure 3.6 is the XRD diagram, which shows the macroscopic structure of GO in the powder or fiber form. The left figure is LGO, and the right is S40. The detailed information of the main peaks reveals how the basal graphitic planes are stacked. The GO powder made from gel indicates sharp diffraction peaks at 2θ position of 11.10° and 9.92°, corresponding to the interlayer spacing of 7.96 A° and 8.91 A°, respectively. After wet-spinning process using CTAB as coagulation agent, the peaks shift toward left with corresponds to enlarged d-spacing. The increase in d-spacing may be due to some CTAB molecules intercalating between the layers. On the other hand, if using NaOH as coagulation agent, the layer-by-layer distance does not change much. This might because sodium hydroxide is small and highly soluble in water. Not many sodium hydroxide molecules participate in intercalate between layers. Hence, the crystalline structure does not change before and after GO-NaOH fiber formation. Scherrer equation is used to calculate the mean of the crystalline domain of the powdered LGO/SGO and the GO-CTAB fiber. Number of crystalline layers is acquired by the quotient of mean size of crystalline domain and interlayer spacing. For both LGO and SGO, GO pristine solutions and GO-NaOH fibers have similar number of crystalline layers. GO-CTAB has only about 10 layers for both cases, which might attribute to the process of ultrasonication which ruin the pristine crystalline structures. Interestingly, there are small but broad peaks for both CTAB-GO cases at 2θ = ~18° but cannot be seen in pristine GO nor GO-NaOH curves. This might be because the formation of the secondary structure of folding or bending of intercalated CTAB or extra random GO sheet wrinkles and crumples caused by CTAB-facilitated self-assembly process.

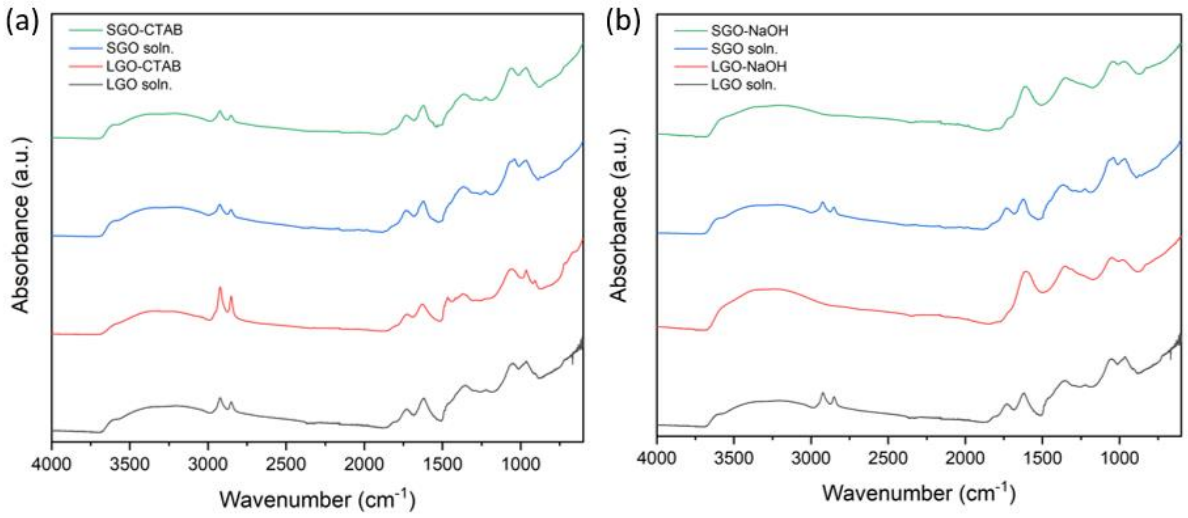

Fig. 3.7. FTIR diagrams for (a) LGO, SGO solution and their fibers in CTAB coagulation bath and (b) LGO, SGO solution and their fibers in NaOH coagulation bath. Pristine GO solutions were freeze overnight and then grinded into powders before conducting FTIR.

From Figure 3.7 (a), the LGO and SGO and GO-CTAB fibers has oxygenated functional groups in its graphitic sheets: carboxyl (COOH), carbonyl (-C=O), and hydroxyl (-OH) groups on the graphene sheet basal plane and edges. There are six main peaks centered at 970, 1040, 1622, 1730, 2852, 2924, and 3220 cm^{-1}. The peak at 1730 and 1622 cm^{-1} arises from the stretching of C=O on carboxyl groups. The two small peaks at 2852 and 2924 cm^{-1} indicates the hydrogen bonded OH groups of dimeric COOH groups and intra-molecular bonded O-H stretching of alcohol respectively. The broad peak at 3220 cm^{-1} indicates the presence of OH stretching in carboxyl (COOH) and hydroxyl (-OH) groups. FT-IR absorption patterns were similar in Figure 3.7 (a). This demonstrates that GO-CTAB fibers preserved the functional groups (hydroxyl and carboxyl group) of the initial GO dispersion, whereas the peaks at 1730, 2852 and 2924 cm^{-1} of GO-NaOH

fibers in 3.7 (b) disappeared, which mean that the strong basic NaOH destroyed the functionality of carboxyl group by deprotonation.

3.3.2 Liquid Crystal

To check if the fiber water redispersions remain the liquid crystallinity, polarized optical microscope is applied.

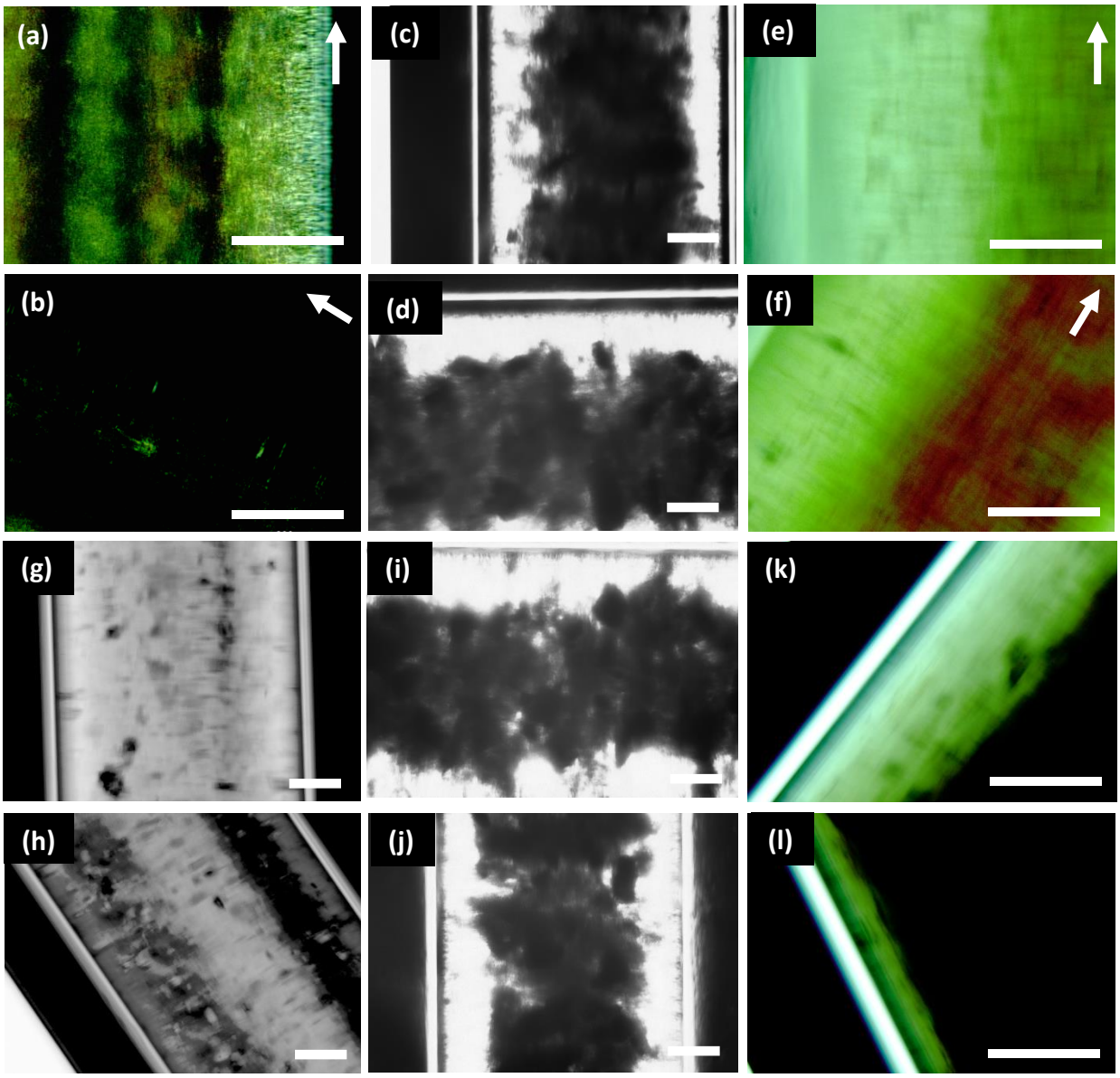

Fig. 3.8. Polarized optical microscope (POM) images of a) b) SGO pristine solution, c) d) SGO-CTAB and e) f) SGO-NaOH fiber re-dispersed solution, g) h) LGO pristine solution, i) j) LGO-CTAB and k) l) LGO-NaOH fiber re-dispersion solution. The GO dispersion samples (2 wt.%) were placed in capillary tubes. The scale bars are all 50 μm. Arrows in the pictures show the direction of the samples.

Figure 3.8 shows polarized optical microscopy (POM) images of the gel-state GO and the solution after re-dispersing the GO powders into water. 3.5(a) indicates polarized light passing through the pristine sample, while the light is blocked when rotating the sample 50 degrees, denoted in (b). This suggests highly ordered GO nematic domains, evidenced by the spreading Schlieren textures[23]. Same birefringence phenomenon is observed for both cases of LGO and SGO pristine solutions. However, the CTAB-GO re-dispersed solution does not display birefringence, i.e. no differences between (c) and (d) or (i) and (j). A possible reason is that GO sheets aggregate into large particles and the aspect ratio is drastically decreased. The decrease of the aspect ratio and the effect of GO aggregation is proved by Keyence confocal laser profilometer shown in S2. According to Onsager's theory, only above certain value of aspect ratio liquid crystals in dispersion can be formed[24]. The challenge is how to exfoliate graphene oxide sheets back to their original state. GO-NaOH fiber, on the other hand, referred (e), (f), (k) and (l), showed massive appearance change. This is because NaOH modified GO sheet with more negatively charged carboxyl groups ($-COO^-$) which created electrostatics repulsion for better redispersion and prevented sheets from aggregation like CTAB did. Therefore, more exfoliated and transparent GO

sheets were preserved. To conclude, both LGO and SGO perform the same way: CTAB makes GO sheets aggregate while NaOH helps the particles stay in liquid crystal.

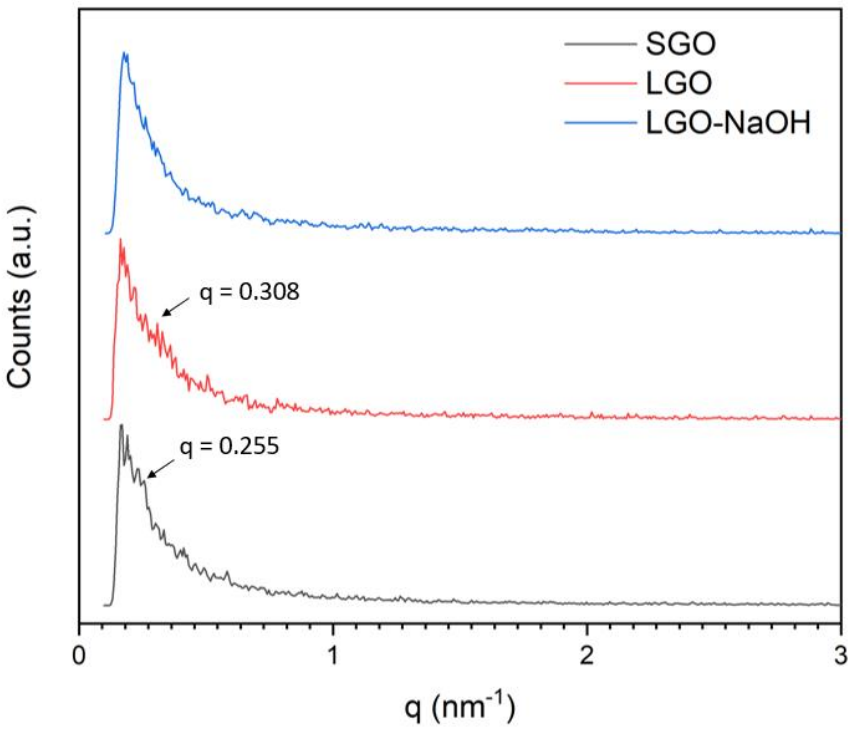

Fig. 3.9. SAXS profile of liquid crystals of GO with high concentrations (mass fraction f_m = 0.02). The spectra depict the scattering intensity as a function of scattering vector q ($q = (4\pi \sin\theta)/\lambda$, where 2θ is the scattering angle).

Polarized optical microscope shows the liquid crystal evidence qualitatively. Small-angle X-ray scattering (SAXS) studies further revealed quantitative structural information of GO dispersions[25]. Figure 3.9 displays the result of SAXS of both LGO and SGO. There are bumps at q = 0.308 and 0.255 nm^{-1} for LGO and SGO curves, which can be transformed into interlayer distance of 20.4 and 27.9 nm, respectively. We therefore propose that the nematic phase of GO should evolve to a lamellar phase that has positional ordering at a higher concentration of GO

sheets. This is quantitative evidence of liquid crystal. Meanwhile, LGO-NaOH curve does not possess such distinct bump. This phenomenon may attribute to the curled sheets that weaken the ordered structure, or the extreme low intensity of X-ray beam compared to synchrotron light source. Besides, the low intensity of X-ray beam results in zigzagging patterns.

3.4. Conclusion

Due to the dramatic mass reduction, the self-assembled GO fibers are much easier and of lower cost method for GO transportation compared to huge volume/mass of GO water dispersions. In addition, the wet-spinning process is easy to scale up. Obtaining a well-dispersed graphene oxide solution from the fabricated graphene oxide fibers is feasible.

A conclusion is drawn that after transforming GO water dispersion into fibers, GO solid could be extracted from bulky gel without altering the physical and chemical structures much. With different coagulation agent, different purpose can be fulfilled. Sodium hydroxide is good at maintaining liquid crystallinity and preventing re-stacking; whereas CTAB is good at retaining chemical properties. This facile method is very promising for GO transportation, as it easily avoids the transportation of the huge volume of water.

Acknowledgment

This work was funded by KISCO Co. in South Korea. The graphene oxide materials were provided by EMD Material Performance Co. and KISCO Co. The material characterizations were obtained via facilities at the Cornell Center for Materials Research, the Cornell Energy Systems Institute,

and Susan Daniel Lab in Chemical Engineering department in Cornell. I also want to thank all the staffs in CCMR and Dr. Jiefu Yin for their kind and knowledgeable help.

REFERENCES

[1] W.S. Hummers, R.E. Offeman, Preparation of Graphitic Oxide, J. Am. Chem. Soc. 80 (1958) 1339. doi:10.1021/ja01539a017.

[2] B.G. Eda, M. Chhowalla, Chemically Derived Graphene Oxide : Towards Large-Area Thin-Film Electronics and Optoelectronics, Adv. Mater. 22 (2010) 2392–2415. doi:10.1002/adma.200903689.

[3] H.A. Becerril, J. Mao, Z. Liu, R.M. Stoltenberg, Z. Bao, Y. Chen, Evaluation of Solution-Processed Reduced Graphene Oxide Films as Transparent Conductors, ACS Nano. 2 (2008) 463–470.

[4] G. Eda, G. Fanchini, M. Chhowalla, Large-area ultrathin films of reduced graphene oxide as a transparent and flexible electronic material, Nat. Nanotechnol. 3 (2008) 270–274. doi:10.1038/nnano.2008.83.

[5] D. Chen, H. Feng, J. Li, Graphene Oxide: Preparation, Functionalization, and Electrochemical Applications, Chem. Rev. 112 (2012) 6027–6053. doi:10.1021/cr300115g.

[6] D.R. Dreyer, H. Jia, C.W. Bielawski, Graphene Oxide : A Convenient Carbocatalyst for Facilitating Oxidation and Hydration Reactions **, Angew. Chemie Int. Ed. 49 (2010) 6813–6816. doi:10.1002/anie.201002160.

[7] B.Y. Song, K. Qu, C. Zhao, J. Ren, X. Qu, Graphene Oxide : Intrinsic Peroxidase Catalytic Activity and Its Application to Glucose Detection, Adv. Mater. 22 (2010) 2206–2210. doi:10.1002/adma.200903783.

[8] Y. Chen, L. Chen, H. Bai, L. Li, Graphene oxide-chitosan composite hydrogels as broad-spectrum adsorbents for water purification, J. Mater. Chem. A. 1 (2013) 1992–2001. doi:10.1039/c2ta00406b.

[9] H.M. Hegab, L. Zou, Graphene oxide-assisted membranes: Fabrication and potential applications in desalination and water purification, J. Memb. Sci. 484 (2015) 95–106. doi:10.1016/j.memsci.2015.03.011.

[10] D. Li, M.B. Müller, S. Gilje, R.B. Kaner, G.G. Wallace, Processable aqueous dispersions of graphene nanosheets, Nat. Nanotechnol. 3 (2008) 101–105. doi:10.1038/nnano.2007.451.

[11] Z. Wang, Y. Dong, H. Li, Z. Zhao, H. Bin Wu, C. Hao, S. Liu, J. Qiu, X.W.D. Lou, Enhancing lithium-sulphur battery performance by strongly binding the discharge products on amino-functionalized reduced graphene oxide, Nat. Commun. 5 (2014) 1–8. doi:10.1038/ncomms6002.

[12] M.F. El-Kady, S. Veronica, D. Sergey, B.K. Richard, Laser Scribing of High-Performance, Science (80-.). 335 (2012) 1326–1330. doi:10.1126/science.1216744.

[13] Y. Li, K. Sheng, W. Yuan, G. Shi, A high-performance flexible fibre-shaped electrochemical capacitor based on electrochemically reduced graphene oxide, Chem. Commun. 49 (2013) 291–293. doi:10.1039/c2cc37396c.

[14] A.A.A. Liela Shahriary, Graphene Oxide Synthesized by using Modified Hummers Approach, Int. J. Renew. Energy Environ. Eng. 02 (2014) 58–63.

[15] O. Akhavan, E. Ghaderi, Toxicity of graphene and graphene oxide nanowalls against bacteria, ACS Nano. 4 (2010) 5731–5736. doi:10.1021/nn101390x.

[16] A.B. Seabra, A.J. Paula, R. De Lima, O.L. Alves, N. Durán, Nanotoxicity of graphene and graphene oxide, Chem. Res. Toxicol. 27 (2014) 159–168. doi:10.1021/tx400385x.

[17] Z. Xu, H. Sun, X. Zhao, C. Gao, Ultrastrong fibers assembled from giant graphene oxide

sheets, Adv. Mater. 25 (2013) 188–193. doi:10.1002/adma.201203448.
[18] J.H. Lee, N. Park, B.G. Kim, D.S. Jung, K. Im, J. Hur, Restacking-Inhibited 3D Reduced Graphene Oxide for High Performance Supercapacitor Electrodes, ACS Nano. 7 (2013) 9366–9374.
[19] H. Wu, W. Lu, J.J. Shao, C. Zhang, M.B. Wu, B.H. Li, Q.H. Yang, pH-dependent size, surface chemistry and electrochemical properties of graphene oxide, Xinxing Tan Cailiao/New Carbon Mater. 28 (2013) 327–335. doi:10.1016/S1872-5805(13)60085-2.
[20] R. Jalili, S.H. Aboutalebi, D. Esrafilzadeh, R.L. Shepherd, J. Chen, S. Aminorroaya-Yamini, K. Konstantinov, A.I. Minett, J.M. Razal, G.G. Wallace, Scalable one-step wet-spinning of graphene fibers and yarns from liquid crystalline dispersions of graphene oxide: Towards multifunctional textiles, Adv. Funct. Mater. 23 (2013) 5345–5354. doi:10.1002/adfm.201300765.
[21] R.L.D. Whitby, A. Korobeinyk, V.M. Gun'Ko, R. Busquets, A.B. Cundy, K. László, J. Skubiszewska-Ziba, R. Leboda, E. Tombacz, I.Y. Toth, K. Kovacs, S. V. Mikhalovsky, PH-driven physicochemical conformational changes of single-layer graphene oxide, Chem. Commun. 47 (2011) 9645–9647. doi:10.1039/c1cc13725e.
[22] D.H. Everett, Basic Principles of Colloid Science, The Royal Society of Chemistry, 1988. doi:10.1039/9781847550200.
[23] J. Nehring, A. Saupe, On the schlieren texture in nematic and smectic liquid crystals, J. Chem. Soc. Faraday Trans. 2 Mol. Chem. Phys. 68 (1972) 1–15. doi:10.1039/F29726800001.
[24] F. Guo, F. Kim, T.H. Han, V.B. Shenoy, J. Huang, R.H. Hurt, Hydration-responsive folding and unfolding in graphene oxide liquid crystal phases, ACS Nano. 5 (2011) 8019–8025. doi:10.1021/nn2025644.
[25] Z. Xu, C. Gao, Aqueous Liquid Crystals of Graphene Oxide, ACS Nano. (2011) 2908–2915. doi:10.1021/nn200069w.

APPENDICES

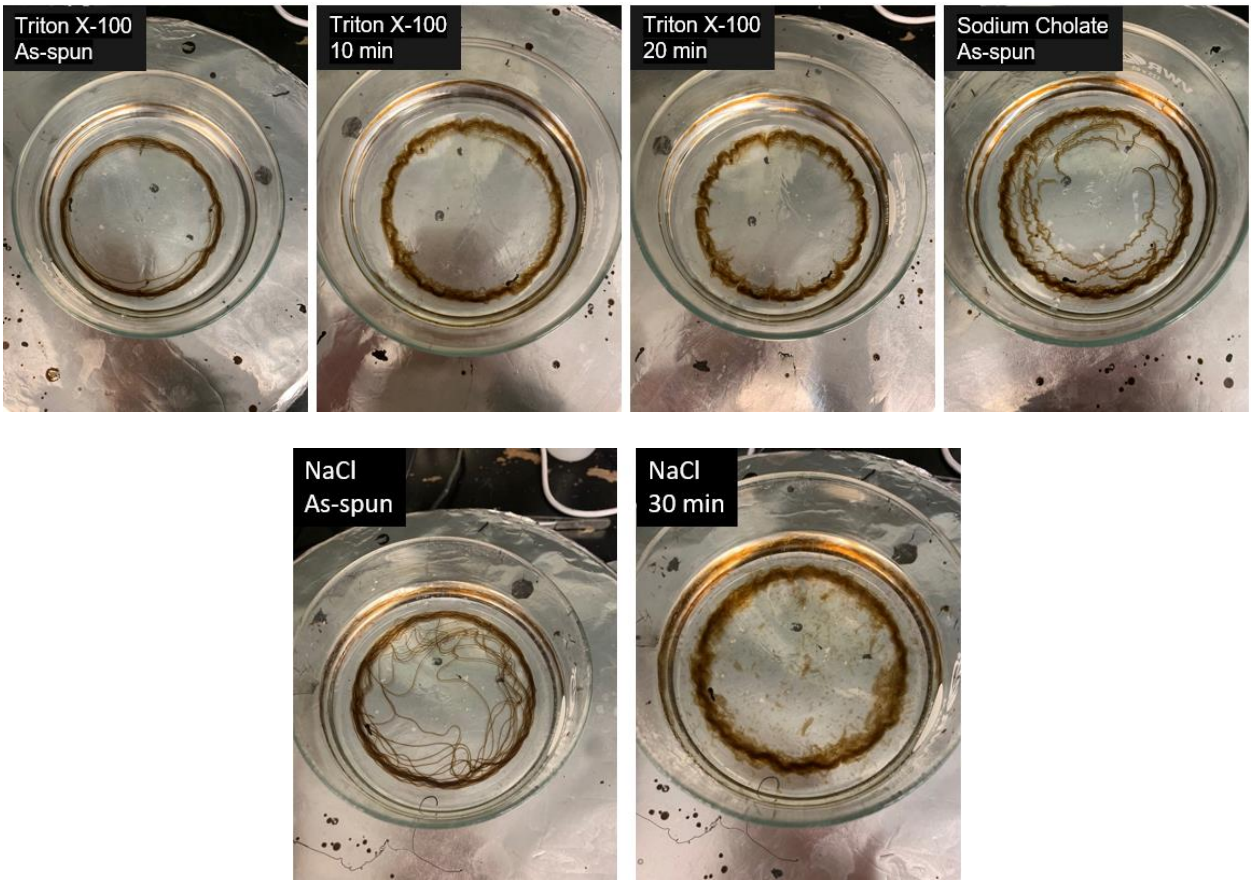

Fig. S1. Images of SGO fiber in weak coagulant (surfactant) bath like Triton X-100, sodium cholate and sodium chloride. Fiber started to disintegrate in a short time and could not be taken out from the bath using a needle.

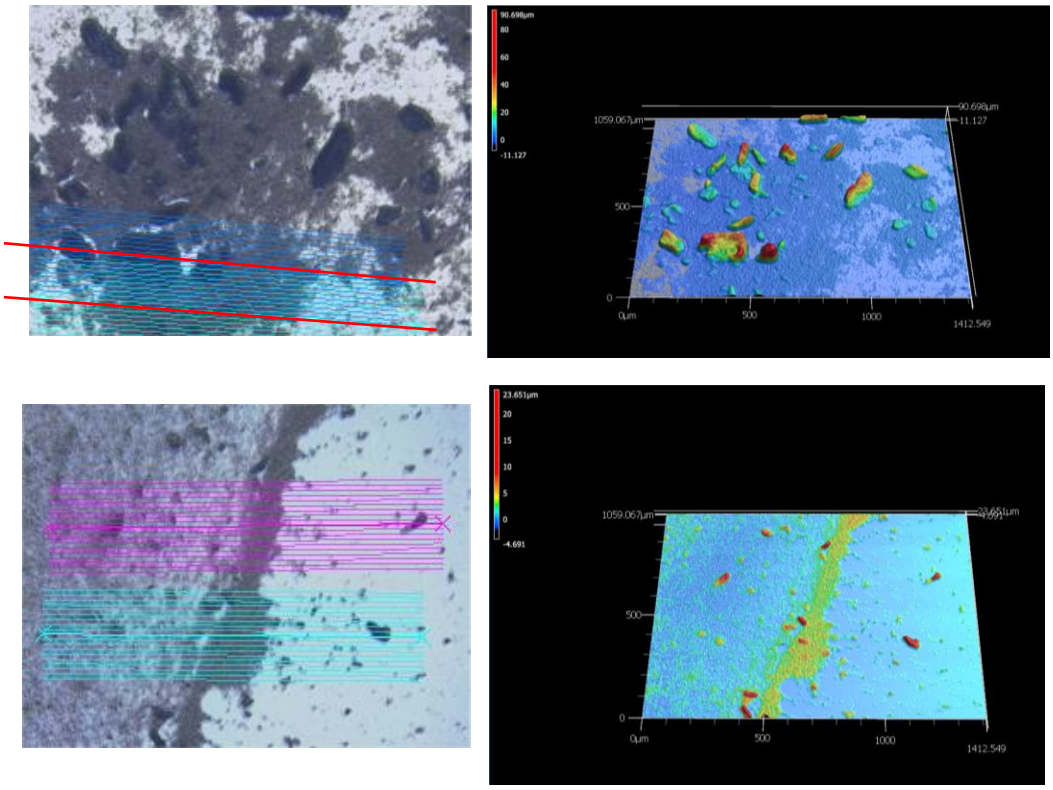

Fig. S2. Keyence confocal microscope showed the surface roughness and particle thicknesses along z axis. The top and bottom are LGO and SGO fiber redispersion using CTAB as coagulant.

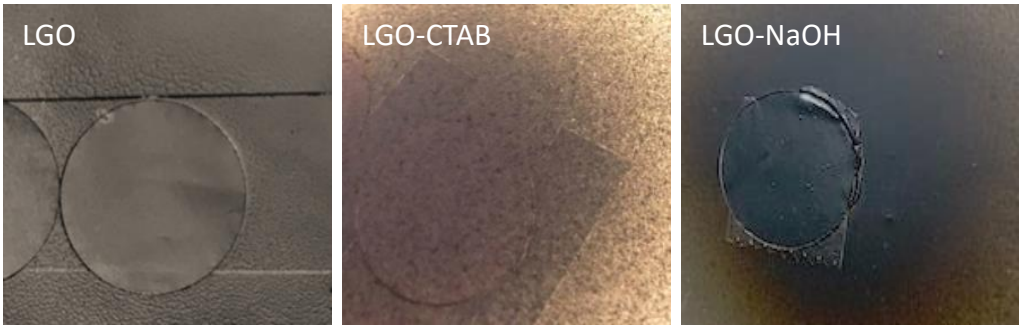

Fig. S3. Images of electrosprayed LGO dispersions.

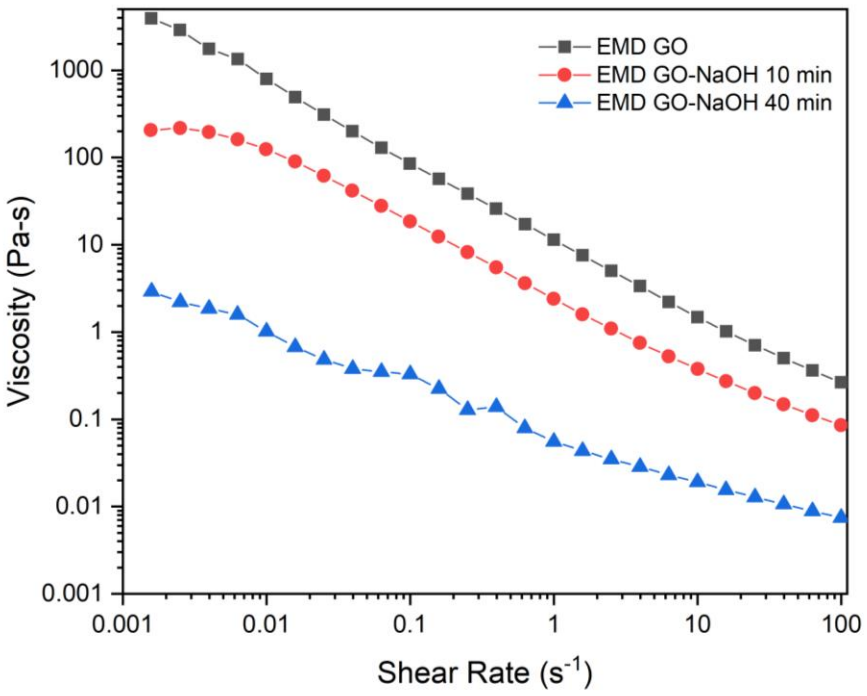

Fig. S4. Relationship between viscosity and shear rate for LGO, LGO fiber dispersion using NaOH as coagulant. The gel fibers were immersed in 1 wt.% NaOH coagulation bath for 10 and 30 minutes before drying and re-dispersing. All the samples possess shear-thinning properties.

CHAPTER 4

Future Work

Although our graphite fibers have extraordinarily high thermal and electrical conductivities, the poor mechanical strength and brittleness are not solid enough to support any applications including lightweight electrical conductors, supercapacitors, solar cells, and so on. Therefore, enhancing mechanical strength as well as elasticity is urgent to be addressed. Literature has shown that adding crosslink agents which connect between graphene flakes is one way to enhance the mechanical strength and toughness. This novel idea is called sequentially bridged graphene. Two types of bridging agents will be investigated to interconnect graphene oxide sheets. 10,12-pentacosadiyn-1-ol attaches to GO sheets' ends by covalent bonding using UV crosslinking; while 1-pyrenebutyric acid N-hydroxysuccinimide ester and 1-aminopyrene attach to sheets by π–π bonding. The reinforced fiber then goes through the same thermal reduction to carbonize. By this approach, mechanical strength is further improved.

In addition, a small amount of polymer like polyacrylonitrile, polyvinyl alcohol, and epoxy can also be doped into the graphene oxide matrix in order to reinforce mechanical strength and flexibility by introducing C-C covalent bonds.

For the water redispersion (Chapter 3), we know that sodium hydroxide serves the purpose of preserving the liquid crystallinity of GO sheet as well as preventing the sheets from restacking. However, because the carboxyl groups of the GO have been deprotonated, conformational changes of the sheets have been triggered. We wonder if anything can be done to reverse the unwanted

consequence of doping sodium hydroxide. For the next step, we will implement sulfuric acid, a common acid for GO preparation, or formic acid, a weak acid, to titrate the pH back to its original acidic state and re-protonate the moieties. Optical microscope and rheometer should be utilized to check if the curled sheet would return to flat sheet just like the pristine GO gel solution. FTIR and XPS should be used to examine whether the functional groups' characteristic peaks could be re-discovered.

Due to time constraint, this project has not been fully explored and some of the scientific reasons behind some results have not been fully explained or proved yet, especially for the mechanism of the conformational change triggered by pH adjustment. Further investigation should be carried out for more comprehensive understanding.